

# Maximal single-frequency electromagnetic response

Zeyu Kuang,<sup>1</sup> Lang Zhang,<sup>1</sup> and Owen D. Miller<sup>1</sup>

<sup>1</sup>*Department of Applied Physics and Energy Sciences Institute,  
Yale University, New Haven, Connecticut 06511, USA*

(Dated: December 21, 2024)

We develop an analytical framework to derive upper bounds to single-frequency electromagnetic response, across near- and far-field regimes, for any materials, naturally incorporating the tandem effects of material- and radiation-induced losses. Our framework relies on a power-conservation law for the polarization fields induced in any scatterer. It unifies previous theories on optical scattering bounds and reveals new insight for optimal nanophotonic design, with applications including far-field scattering, near-field local-density-of-states engineering, and the design of perfect absorbers. For the latter case, our bounds predict strikingly large minimal thicknesses for arbitrarily patterned perfect absorbers, ranging from 50–100 nm for typical materials at visible wavelengths to  $\mu\text{m}$ -scale thicknesses for polar dielectrics at infrared wavelengths. We discover metasurface structures approaching the perfect-absorber bounds through the use of inverse design. More generally, our bounds for arbitrary linear and quadratic electromagnetic response functions apply to objectives such as field-correlation functions, near-field radiative heat transfer, optical force and torque, and arbitrary nanophotonic mode coupling.

## I. INTRODUCTION

Electromagnetic scattering at a single frequency is constrained by two loss mechanisms: material dissipation (absorption) and radiative coupling (scattering). There has been substantial research probing the limits of light-matter interactions subject to constraint of either mechanism [1–21], yet no general theory simultaneously accounting for both. In this Article, we develop a framework for upper bounds to electromagnetic response, across near- and far-field regimes, for any materials, naturally incorporating the tandem effects of material- and radiation-induced losses. Our framework relies on a power-conservation law for the polarization currents induced in any medium via a volume-integral version of the optical theorem [22–25]. An illustrative example is that of plane-wave scattering, where our bounds unify two previously separate approaches: radiative-coupling constraints leading to maximum cross-sections proportional to the square wavelength [1–6],  $\max \sigma \sim \lambda^2$ , and material-dissipation constraints leading to cross-section bounds inversely proportional to material loss [7–9],  $\max \sigma \sim |\chi|^2 / \text{Im } \chi$ . Our framework contains more than a dozen previous results [1–5, 7–9, 11, 12, 14–17] as asymptotic limits, it regularizes unphysical divergences in these results, and it reveals new insight for optimal nanophotonic design, with applications including far-field scattering, near-field local-density-of-states engineering, and the design of perfect absorbers. The ramifications of our bounds for perfect absorbers are striking: we prove that independent of the geometric patterning, the minimum thickness of perfect or near-perfect absorbers comprising conventional materials is typically on the order of 50–100 nm at visible wavelengths, and closer to  $1 \mu\text{m}$  at infrared wavelengths where polar-dielectric materials are resonant. These values are larger than the material skin depths, and roughly  $100\times$  larger than suggested by previous material-loss bounds [7]. We use inverse design to

discover ultrathin absorber designs closely approaching the bounds. The framework developed here has immediate applicability to *any* linear and quadratic response functions in electromagnetic scattering problems, including those that arise in near-field radiative heat transfer (NFRHT) [26–28], optical force/torque [14, 29–32], and more general nanophotonic mode coupling [33].

For many years, there was a single “channel bound” approach underlying the understanding of maximal single-frequency electromagnetic response [1–6, 10–12, 14, 15, 20]. The approach identifies “channels” (typically infinite in number) that carry power towards and away from the scattering body [34–37], use intuition or asymptotic arguments to restrict the scattering process to a finite number of channels, and then apply energy-conservation within those channels to arrive at maximal power-exchange quantities. The canonical example is in bounds for scattering cross-sections, i.e., the total scattered power divided by the intensity of an incoming plane wave. It has long been known that the maximal cross-section of a subwavelength electric-dipole antenna [38], or even a single two-level atomic transition [39], is proportional to the square wavelength; for scattering cross-sections, the bound is  $\sigma_{\text{scat}} \leq 3\lambda^2/2\pi$ . These bounds are consequences of properties of the incident waves (*not* the scatterers): though plane waves carry infinite total power, they carry a finite amount of power in each vector-spherical-wave basis function, and  $3\lambda^2/2\pi$  scattering corresponds simply to scattering all of the power in the electric-dipole channel. Related arguments can be used to bound NFRHT rates, which are constrained by restricting near-field coupling to only finite-wavenumber evanescent waves [10], absorption rates in ultrathin films, which are constrained by symmetry to have nonzero coupling to up/down plane-wave channels [11], and maximal antenna directivity [6]. All such channel bounds are consequences of radiative-coupling constraints, with optimal power-flow dynamics corresponding to ideal coupling to every channel that in-

interacts with the scattering system. The drawbacks of channel bounds are two-fold: (1) they do not account for absorptive losses in the scatterers, and (2) except in the simplest (e.g. dipolar) systems, it is typically impossible to predict *a priori* how many channels may actually contribute in optimal scattering processes. Without any such restrictions, the bounds diverge.

In recent years, an alternative approach has been developed: material-absorption bounds [7–9, 13, 15–21] that rectify the two drawbacks of the channel approaches. These bounds identify upper limits to responses including cross-sections [7], local density of states [19], NFRHT [13], and 2D-material response [8] that are determined by the lossiness of the material comprising the scattering body. The independence from channels provides generality and convenience, but with the key drawback that they do not account for necessary radiative damping. Very recently, for the special case of incoherent thermal or zero-point-field excitations, radiative and absorptive losses are separately identified using the  $\mathbb{T}$  operator, yielding upper bounds for incoherent response functions [40–42].

In this work, we identify a *single* constraint that incorporates the cooperative effects of absorptive and radiative losses at any level of coherence. The constraint is the volume-integral formulation of the optical theorem (Sec. II), which is an energy-conservation constraint that imposes the condition that absorption plus scattered power equal extinction, for any incident field. Channel bounds distill in essence to loosening this constraint to an inequality that scattered power is bounded above by extinction. Material-absorption bounds distill to loosening the optical-theorem constraint to an inequality that absorbed power is bounded above by extinction. Our key innovation is the recognition that one can retain the entire constraint, and enforce the requirement that the sum of absorption and scattered power equal extinction. We describe the use of Lagrangian duality to solve the resulting optimization problems (Sec. IIb), ultimately yielding very general bounds to arbitrary response functions (Sec. IIb,IIc). For the important case of plane-wave scattering (Sec. III), we derive explicit bound expressions and also identify an important application: perfect absorbers. We show that our framework enables predictions of the minimal scatterer thicknesses at which perfect or near-perfect absorption are possible, thicknesses much larger than any previous framework predicted. For thermal absorption/emission applications (Sec. IV), we show that our bounds tighten those of Ref. [40]. In the final section (Sec. V), we discuss the simplicity with which our framework can be applied to numerous other scenarios, and discuss remaining open problems.

## II. GENERAL FORMALISM

Our central finding is a set of upper bounds to maximal single-frequency response. The problem of interest

is to optimize any electromagnetic response function  $f$  subject only to Maxwell’s equations, while allowing for arbitrary patterning within a prescribed region of space. However, Maxwell’s equations represent a nonconvex and highly complex constraint for which global bounds are not known. Instead, we use the optical theorem, and in particular a volume-integral formulation of the optical theorem, as a simple quadratic constraint for which global bounds can be derived. We start with the volume-integral version of Maxwell’s equations, which provide a simple and direct starting point to derive the optical theorem (Sec. IIA). The optical-theorem constraint is quadratic, and we discuss how many previous result can be derived from weaker forms of the constraint. Then in Sec. IIB we use the formalism of Lagrangian duality to derive a single general bound expression, Eq. (6), from which many specialized results follow. In Sec. IIC we consider canonical electromagnetic response functions: absorption, scattering, extinction, and local density of states. Throughout, for compact general expressions, we use six-vector notation with Greek letters denoting vectors and tensors:  $\psi$  for fields,  $\phi$  for polarization currents,  $\chi$  for the susceptibility tensor (which in its most general form can be a nonlocal, inhomogeneous, bianisotropic,  $6 \times 6$  tensor operator [43]). Throughout the letter, we use dimensionless units for which the vacuum permittivity and permeability equal 1,  $\varepsilon_0 = \mu_0 = 1$ . The six-vector fields and polarization currents are given by

$$\psi = \begin{pmatrix} \mathbf{E} \\ \mathbf{H} \end{pmatrix}, \quad \phi = \begin{pmatrix} \mathbf{P} \\ \mathbf{M} \end{pmatrix}. \quad (1)$$

### A. Optical Theorem Constraint

The optical theorem manifests energy conservation: the total power taken from an incident field must equal the sum of the powers absorbed and scattered. As discussed below, the key version of the optical theorem that enables a meaningful constraint is the version that arises from the volume equivalence principle. This principle enables the transformation of the differential Maxwell equations to a volume-integral form. It states that any scattering problem can be separated into a background material distribution (not necessarily homogeneous), and an additional distributed “scatterer” susceptibility. The total fields  $\psi$  are given by the fields incident within the background,  $\psi_{\text{inc}}$ , plus scattered fields  $\Gamma_0 \phi$  that arise from polarization currents  $\phi$  induced in the volume of the scatterer, where  $\Gamma_0$  is the background-Green’s-function convolution operator. For simplicity in the optical theorem below, we define a variable  $\xi$  that is the negative inverse of the susceptibility operator,  $\xi = -\chi^{-1}$ . With this notation, the statement that the total field equals the sum of the incident and scattered fields can be written:  $-\xi \phi = \psi_{\text{inc}} + \Gamma_0 \phi$ . Rearranging to have the unknown variables on the left-hand side and the known variables

on the right-hand side yields the volume-integral equation (VIE),

$$[\Gamma_0 + \xi] \phi = -\psi_{\text{inc}}. \quad (2)$$

We generally allow for  $\chi$  to be nonlocal, as arises in the extreme near field [44] and in 2D materials [45]; when  $\chi$  is local and can be written  $\chi(\mathbf{x}, \mathbf{x}') = \chi(\mathbf{x})\delta(\mathbf{x} - \mathbf{x}')$ , Eq. (2) becomes a standard VIE [43]:  $\int_V \Gamma_0(\mathbf{x}, \mathbf{x}')\phi(\mathbf{x}')d\mathbf{x}' - \chi^{-1}(\mathbf{x})\phi(\mathbf{x}) = -\psi_{\text{inc}}(\mathbf{x})$ , where  $V$  is the volume of the scatterer.

The volume-integral-equation optical theorem can be derived from Eq. (2) by taking the inner product of Eq. (2) with  $\phi$  (denoted  $\phi^\dagger$ ), multiplying by  $\omega/2$ , and taking the imaginary part of both sides of the equation, yielding:

$$\underbrace{\frac{\omega}{2}\phi^\dagger (\text{Im } \Gamma_0) \phi}_{P_{\text{scat}}} + \underbrace{\frac{\omega}{2}\phi^\dagger (\text{Im } \xi) \phi}_{P_{\text{abs}}} = \underbrace{\frac{\omega}{2}\text{Im} \left( \psi_{\text{inc}}^\dagger \phi \right)}_{P_{\text{ext}}}, \quad (3)$$

where the inner product is the integral over the volume of the scatterer. Within the optical theorem of Eq. (3), we identify the three terms as scattered, absorbed, and extinguished power, respectively [46, 47], as depicted in Fig. 1. The operator  $\text{Im } \Gamma_0$  represents power radiated into the background, into near-field or, more typically, far-field scattering channels. For any background materials,  $\text{Im } \Gamma_0$  can be computed by standard volume-integral (or discrete-dipole-approximation) techniques [43, 48], and when the background is lossless over the scatterer domain it is nonsingular and simpler to compute [49]. In vacuum, the operator can be written analytically for high-symmetry domains. It is a positive semidefinite operator because the power radiated by any polarization currents must be nonnegative in a passive system. The second term with  $\text{Im } \xi$  represents absorbed power: work done by the polarization currents on the total fields. In terms of the susceptibility,  $\text{Im } \xi = \chi^{-1} (\text{Im } \chi) (\chi^\dagger)^{-1}$ ; for scalar material permittivities, it simplifies to  $\text{Im } \chi/|\chi|^2$ , which is the inverse of a material “figure of merit” that has appeared in many material-loss bounds [7, 8, 19]. The operator  $\text{Im } \xi$  is positive definite for any material without gain [43, 50]. Finally, the third term is the imaginary part of the overlap between the incident field and the induced currents, which corresponds to extinction (total power taken from the incident fields).

Equation (3) has three key features: (1) it contains *both* the powers radiated ( $P_{\text{scat}}$ ) and absorbed ( $P_{\text{abs}}$ ) by the polarization currents in a single expression, (2) it is a quadratic constraint that is known to have “hidden” convexity for any quadratic objective function [51], and (3) it incorporates information about the material composition of the scatterer, and possibly a bounding volume containing it, while independent of any other patterning details.

The optical-theorem constraint of Eq. (3) constrains the polarization-current vector  $\phi$  to lie on the surface of a high-dimensional ellipsoid whose principal axes are

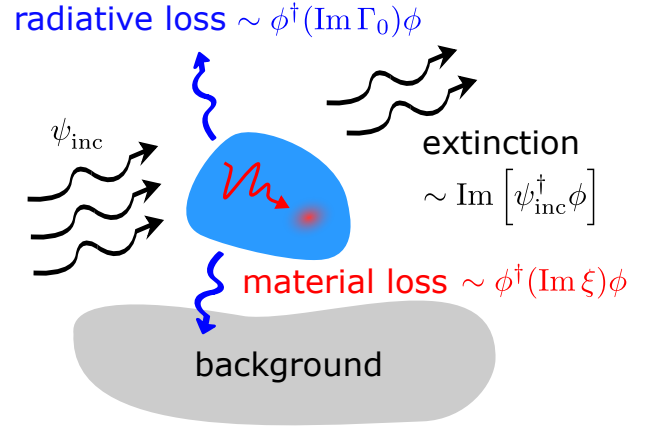


FIG. 1. Illustration of the two loss mechanisms in electromagnetic scattering. An incident field  $\psi_{\text{inc}}$  induces polarization currents  $\phi$  in the scatterer. Energy dissipated inside the material corresponds to material loss, determined by operator  $\text{Im } \xi = \chi^{-1} (\text{Im } \chi) (\chi^\dagger)^{-1}$  for susceptibility  $\chi$ . Energy coupled to the background, into far-field or near-field power exchange, corresponds to radiative loss, determined by the operator  $\text{Im } \Gamma_0$ . Total extinction is the sum of the two and is linear in  $\phi$ , as dictated by the optical theorem.

the eigenvectors of  $\text{Im } \Gamma_0 + \text{Im } \xi$  and whose radii are constrained by the norm of  $\psi_{\text{inc}}$ . In the SM we show that all previous channel or material-loss bounds discussed in the Introduction can be derived by applying weaker versions of Eq. (3). Channel bounds can be derived by loosening Eq. (3) to the inequality  $P_{\text{scat}} \leq P_{\text{ext}}$ , without the absorption term (but implicitly using the fact that absorbed power is nonnegative). Material-loss bounds can be derived by loosening Eq. (3) to the inequality  $P_{\text{abs}} \leq P_{\text{ext}}$ , without the scattered-power term (but using the fact that scattered power is nonnegative). Of course, including both constraints simultaneously can only result in equal or tighter bounds.

## B. General Formalism

Any electromagnetic power-flow objective function  $f$  is either linear or quadratic in the polarization currents  $\phi$ , and can be generically written as  $f(\phi) = \phi^\dagger \mathbb{A} \phi + \text{Im}(\beta^\dagger \phi)$ , where  $\mathbb{A}$  is a self-adjoint operator and  $\beta$  is any six-vector field on the scatterer domain. Then the maximal  $f$  that is possible for any scatterer is given by the optimization problem:

$$\begin{aligned} \max_{\phi} \quad & f(\phi) = \phi^\dagger \mathbb{A} \phi + \text{Im}(\beta^\dagger \phi) \\ \text{s.t.} \quad & \phi^\dagger \{ \text{Im } \xi + \text{Im } \Gamma_0 \} \phi = \text{Im}(\psi_{\text{inc}}^\dagger \phi). \end{aligned} \quad (4)$$

This is a quadratic objective with a single quadratic constraint, which is known to have strong duality [52]. If we follow standard convex-optimization conventions and consider as our “primal” problem that of Eq. (4), but instead written as a minimization over the negative of  $f(\phi)$ ,

then strong duality implies that the maximum of the corresponding Lagrangian dual functions equals the minimum of the primal problem, and thus the maximum of Eq. (4). By straightforward calculations, the dual function is

$$g(\nu) = \begin{cases} -\frac{1}{4}(\beta + \nu\psi_{\text{inc}})^\dagger \mathbb{B}^{-1}(\nu)(\beta + \nu\psi_{\text{inc}}) & \nu > \nu_0 \\ -\infty, & \nu < \nu_0 \end{cases} \quad (5)$$

where  $\nu$  is the dual variable,  $\mathbb{B}(\nu) = -\mathbb{A} + \nu(\text{Im } \xi + \text{Im } \Gamma_0)$  and  $\nu_0$  is the value of  $\nu$  for which the minimum eigenvalue of  $\mathbb{B}(\nu_0)$  is zero. (The definiteness of  $\text{Im } \Gamma_0$  and  $\text{Im } \xi$  ensure there is only one  $\nu_0$ , cf. SM.) At  $\nu = \nu_0$ , some care is needed to evaluate  $g(\nu_0)$  because the inverse of  $\mathbb{B}(\nu_0)$  does not exist (due to the 0 eigenvalue). If  $\beta + \nu_0\psi_{\text{inc}}$  is in the range of  $\mathbb{B}(\nu_0)$ , then  $g(\nu_0)$  takes the value of the first case in Eq. (5) with the inverse operator replaced by the pseudo-inverse; if not, then  $g(\nu_0) \rightarrow -\infty$ . (Each scenario arises in the examples below.) By the strong duality of Eq. (4), the optimal value of the dual function, Eq. (5), gives the optimal value of the “primal” problem, Eq. (4) (accounting for the sign changes in converting the maximization to minimization). In the SM we identify the only two possible optimal values of  $\nu$ :  $\nu_0$ , defined above, or  $\nu_1$ , which is the stationary point for  $\nu > \nu_0$  at which the derivative of  $g(\nu)$  equals zero. Denoting this optimal value  $\nu^*$ , we can write the maximal response as:

$$f_{\text{max}} = \frac{1}{4}(\beta + \nu^*\psi_{\text{inc}})^\dagger [-\mathbb{A} + \nu^*(\text{Im } \xi + \text{Im } \Gamma_0)]^{-1} (\beta + \nu^*\psi_{\text{inc}}) \quad (6)$$

Although Eq. (6) may appear abstract, it is a general bound that applies for any linear or quadratic electromagnetic response function, from which more domain-specific specialized results follow.

### C. Power quantities and LDOS

If one wants to maximize one of the terms already present in the constraint, i.e. absorption, scattered power, or extinction, then the  $\mathbb{A}$  and  $\beta$  terms take particularly simple forms (cf. SM), leading to the bounds:

$$P_{\text{ext}} \leq \frac{\omega}{2} \psi_{\text{inc}}^\dagger (\text{Im } \xi + \text{Im } \Gamma_0)^{-1} \psi_{\text{inc}} \quad (7)$$

$$P_{\text{abs}} \leq \frac{\omega}{2} \frac{\nu^{*2}}{4} \psi_{\text{inc}}^\dagger [(\nu^* - 1) \text{Im } \xi + \nu^* \text{Im } \Gamma_0]^{-1} \psi_{\text{inc}} \quad (8)$$

$$P_{\text{scat}} \leq \frac{\omega}{2} \frac{\nu^{*2}}{4} \psi_{\text{inc}}^\dagger [\nu^* \text{Im } \xi + (\nu^* - 1) \text{Im } \Gamma_0]^{-1} \psi_{\text{inc}}. \quad (9)$$

where  $\nu^*$  is the dual-variable numerical constant (SM).

Bounds on LDOS represent maximal spontaneous-emission enhancements [53–57]. Total (electric) LDOS,  $\rho_{\text{tot}}$ , is proportional to the averaged power emitted by three orthogonally polarized and uncorrelated unit electric dipoles [58–61]. It can be separated into a radiative part,  $\rho_{\text{rad}}$ , for far-field radiation, and a non-radiative

part,  $\rho_{\text{nr}}$ , that is absorbed by the scatterer [22]. Exact but somewhat cumbersome LDOS bounds for arbitrary materials are derived from Eq. (6) in the SM; for nonmagnetic materials, the bounds simplify to expressions related to the maximum power quantities given in Eqs. (7)–(9):

$$\rho_{\text{tot}} \leq \frac{2}{\pi\omega^2} \sum_j P_{\text{ext},j}^{\text{max}} + \rho_0 \quad (10)$$

$$\rho_{\text{nr}} \leq \frac{2}{\pi\omega^2} \sum_j P_{\text{abs},j}^{\text{max}} \quad (11)$$

$$\rho_{\text{rad}} \leq \frac{2}{\pi\omega^2} \sum_j P_{\text{sca},j}^{\text{max}} + \rho_0, \quad (12)$$

where  $\rho_0$  is the electric LDOS of the background material, and takes the value of  $\frac{\omega^2}{2\pi^2 c^3}$  for a scatterer in vacuum [62]. The summation over  $j = 1, 2, 3$  accounts for three orthogonally polarized unit dipoles. As shown in the SM, our bound is tighter than previous bounds on LDOS [7]. In the extreme near field, where material loss dominates, our bound agrees with the known material-loss bound [7].

The bounds of Eqs. (6)–(12) are sufficiently general to allow for arbitrary material composition (inhomogeneous, nonlocal, etc.), in which case the bounds require computations involving the  $\text{Im } \Gamma_0$  and  $\text{Im } \xi$  matrices. In the SM, we provide a sequence of simplifications, showing step-by-step the increasingly simplified bounds that arise under restrictions of the incident field, material, or bounding volumes involved. In the next section, we consider the important case in which a plane wave is incident upon an isotropic nonmagnetic medium.

## III. PLANE-WAVE SCATTERING

A prototypical scattering problem is that of a plane wave in free space incident upon an isotropic (scalar susceptibility), nonmagnetic scatterer. The assumption of a scalar susceptibility introduces important simplifications into the bounds. The operator  $\text{Im } \xi$  is then a scalar multiple of the identity matrix  $\mathbb{I}$ ,

$$\text{Im } \xi = \frac{\text{Im } \chi}{|\chi|^2} \mathbb{I}, \quad (13)$$

and is therefore diagonal in any basis that diagonalizes  $\text{Im } \Gamma_0$ , simplifying the matrix-inverse expressions in the bounds of Eqs. (6)–(12). For nonmagnetic materials, the polarization currents  $\phi$  comprise nonzero electric polarization currents  $\mathbf{P}$  only, such that the  $6 \times 6$  Green’s tensor  $\Gamma_0$  can be replaced by its  $3 \times 3$  electric-field-from-electric-current sub-block  $\mathbb{G}_0^{\text{EE}}$ , and only the electric part  $\mathbf{E}_{\text{inc}}$  of the incident field  $\psi_{\text{inc}}$  enters the bounds of Eqs. (7)–(9). Because  $\text{Im } \mathbb{G}_0^{\text{EE}}$  is positive-definite, we can simplify its eigendecomposition to write  $\text{Im } \mathbb{G}_0^{\text{EE}} = \mathbb{V} \mathbb{V}^\dagger$ , where the columns of  $\mathbb{V}$ , which we denote  $\mathbf{v}_i$ , form an orthogonal



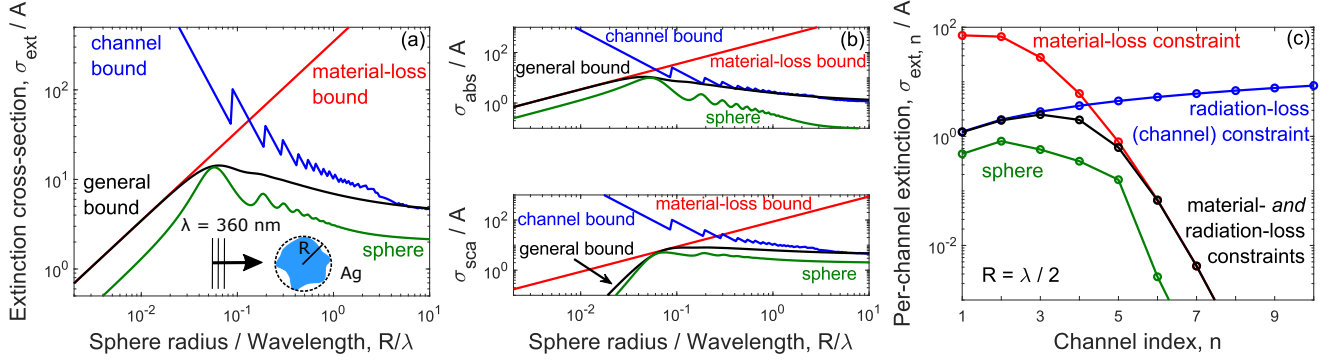


FIG. 2. Plane wave of wavelength  $\lambda = 360$  nm scattering from a finite Ag [63] scatterer, enclosed by a spherical bounding volume with radius  $R$ . The channel bound is heuristically regularized by ignoring small-scattering high-order channels. All cross-sections are normalized by geometric cross-section  $A$ . (a). Bound of extinction cross-section for different  $R$ . The general bound regularizes divergence in previous bounds and are tighter for wavelength-scale sizes. (b) Similar behavior is observed in the bounds for scattering and absorption cross-sections. (c) Per-channel extinction cross section  $\sigma_{\text{ext},n}$  (defined in SM) for  $R = \lambda/2$ . Low-order scattering channels are dominated by radiative loss, while high-order scattering channels are dominated by material loss.

basis of polarization currents. They are normalized such that the set of  $\mathbf{v}_i^\dagger \mathbf{v}_i$  are the eigenvalues of  $\text{Im } \mathbb{G}_0^{\text{EE}}$  and represent the powers radiated by unit-normalization polarization currents. More simply, the  $\mathbf{v}_i$  span the space of scattering channels and the eigenvalues  $\rho_i$  represent corresponding radiated powers.

An incident propagating plane wave (or any wave incident from the far field, cf. SM) can be decomposed in the basis  $\mathbb{V}$ . We write the expansion as  $\mathbf{E}_{\text{inc}} = \frac{1}{k^{3/2}} \sum_i e_i \mathbf{v}_i$ , where the  $e_i$  are the expansion coefficients, and we factor out the free-space wavenumber  $k$  to simplify the expressions below. Inserting the eigendecomposition of  $\text{Im } \mathbb{G}_0^{\text{EE}}$  and the plane-wave expansion in this basis into Eqs. (7)–(9) gives general power bounds for plane-wave scattering:

$$P_{\text{ext}} \leq \frac{\lambda^2}{8\pi^2} \sum_i |e_i|^2 \frac{\rho_i}{\text{Im } \xi + \rho_i} \quad (14)$$

$$P_{\text{abs}} \leq \frac{\lambda^2}{8\pi^2} \frac{\nu^{*2}}{4} \sum_i |e_i|^2 \frac{\rho_i}{(\nu^* - 1) \text{Im } \xi + \nu^* \rho_i} \quad (15)$$

$$P_{\text{sca}} \leq \frac{\lambda^2}{8\pi^2} \frac{\nu^{*2}}{4} \sum_i |e_i|^2 \frac{\rho_i}{\nu^* \text{Im } \xi + (\nu^* - 1) \rho_i}. \quad (16)$$

The variable  $\nu^*$  is the optimal dual variable discussed above; its value can be found computationally via a transcendental equation given in the SM. The bounds of Eqs. (14)–(16) naturally generalize previous channel bounds ( $\sim \lambda^2$ ) and material-absorption bounds ( $\sim 1/\text{Im } \xi = |\chi|^2/\text{Im } \chi$ ); in the SM, we prove that removing either dissipation pathway results in the previous expressions.

The bounds of Eqs. (14)–(16) require knowledge of the eigenvalues of  $\text{Im } \mathbb{G}_0^{\text{EE}}$ , and thus the exact shape of the scattering body, to compute the values of  $\rho_i$ . However, analytical expressions for  $\rho_i$  are known for high-symmetry geometries, and a useful property of the optimization problem of Eq. (4) is that its value is bounded

above by the same problem embedded in a larger bounding domain. (It is always possible for the currents in the “excess” region to be zero.) In the following two subsections we consider the two possible scenarios one can encounter: (a) scattering by finite-sized objects, which can be enclosed in spherical bounding surfaces, and (b) scattering by extended (e.g. periodic) objects, which can be enclosed in planar bounding surfaces.

### A. Finite-sized scatterers

Finite-sized scatterers can be enclosed by a minimal bounding sphere with radius  $R$ , as in the inset of Fig. 2(a). The basis functions  $\mathbf{v}_i$  are vector spherical waves (VSWs), representing orthogonal scattering channels, with exact expressions given in the SM. The state labels  $i$  can be indexed by the triplet  $i = \{n, m, j\}$  where  $n = 1, 2, \dots$  is the total angular momentum,  $m = -n, \dots, n$  is the  $z$ -directed angular momentum, and  $j = 1, 2$  labels two polarizations. In this basis the expansion coefficients of a plane wave are given by  $|e_i|^2 = \pi(2n+1)\delta_{m,\pm 1}|E_0|^2$ , where  $E_0$  is the plane-wave amplitude. We show in the SM that the values  $\rho_i$  are given by integrals of spherical Bessel functions. With these expressions, bounds for extinction, scattering, and absorption cross-sections are easily determined from Eqs. (14)–(16) after normalization by plane wave intensity  $|E_0|^2/2$ .

In Fig. 2, we compare cross-section bounds derived from Eqs. (14)–(16) to the actual scattering properties of a silver sphere (permittivity data from Ref. [63]) at wavelength  $\lambda = 360$  nm, near its surface-plasmon resonance. We also include the previously derived channel [4] and material-absorption [7] bounds for comparison, and in each case one can see that our general bounds are significantly “tighter” (smaller) than the previous bounds, except in the expected small- and large-size asymptotic

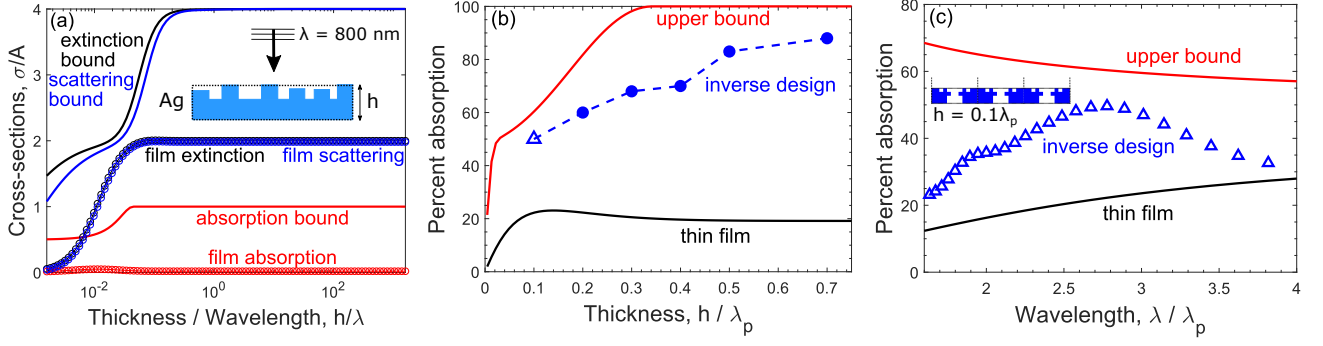


FIG. 3. (a) Plane wave at normal incidence and wavelength  $\lambda = 800$  nm scattering from an extended Ag scatterer, enclosed by a bounding film with thickness  $h$ . Shown here are the bound for extinction, scattering, absorption, compared with scattering quantities for a planar Ag [63] film. (b) Inverse-designed Drude-metal metasurface (plasma wavelength  $\lambda_p$ ) at different thicknesses for maximum absorption at wavelength  $2.75\lambda_p$ , alongside its thin film counterpart and the global absorption bound. (c) Absorption spectrum of ultra-thin absorbers from (b) with thickness  $h = 0.1\lambda_p$ . At the target wavelength, the absorption of the inverse-designed structure is more than double that of the thin film, and reaches 82% of the bound.

limits. At a particular radius, the scattering response even reaches the general bound. In Fig. 2(c), we fix the radius at a half-wavelength and depict the per-channel contributions to the extinction bounds in the radiation-loss-only, material-loss-only, and tandem-loss constraint cases. Higher-order channels have increasingly smaller radiative losses (causing unphysical divergences discussed below), such that material loss is the dominant dissipation channel. Conversely, material-loss-only constraints are inefficient for lower-order channels where radiative losses dominate. Incorporating both loss mechanisms removes the unphysical divergence, accounts for radiative losses, and sets the tightest bound among the three across all channels.

Technically, the channel bound diverges for any finite-sized scatterer, and the blue solid line in Fig. 2(a) should be infinitely high. To obtain a reasonable finite value, we only incorporate channels for which the sphere scattering contributions are greater than 1% of the maximal response, resulting in the step-like behavior seen in the figure. Yet requiring knowledge of the specific scattering structure to compute the upper limit highlights a key drawback of the channel bounds. Moreover, in the large-size limit, there are cumulatively large contributions from many small-scattering channels, such that this cut-off approach results in inaccurate *underestimates* of the cross-sections, and thus invalid bounds unless material loss is included.

## B. Extended scatterers

The second possible scenario is scattering from an infinitely extended (e.g. periodic) scatterer. Such scatterers can always be enclosed by a minimal planar “film” bounding volume with thickness  $h$ , as in the inset of Fig. 3(a). Then the basis functions  $\mathbf{v}_i$  of  $\text{Im}\mathbb{G}_0^{\text{EE}}$  are known to be propagating plane waves with wave vector

$\mathbf{k} = k_x\hat{\mathbf{x}} + k_y\hat{\mathbf{y}} + k_z\hat{\mathbf{z}}$ . Now the index  $i$  maps to the triplet  $i = \{s, p, \mathbf{k}_\parallel\}$ , where  $s = \pm$  denotes even and odd modes,  $p = M, N$  denotes TE and TM polarizations, and  $\mathbf{k}_\parallel = k_x\hat{\mathbf{x}} + k_y\hat{\mathbf{y}}$  denotes the surface-parallel wave vector. In the SM we provide the expressions for  $\mathbf{v}_i$ , and show that the eigenvalues  $\rho_i$  are given by

$$\rho_{\pm, s}(\mathbf{k}_\parallel) = \begin{cases} \frac{k^2 h}{4k_z} (1 \pm \frac{\sin(k_z h)}{k_z h}) & s = \text{TE} \\ \frac{k^2 h}{4k_z} (1 \pm \frac{\sin(k_z h)}{k_z h}) \mp \frac{\sin(k_z h)}{2} & s = \text{TM} \end{cases} \quad (19)$$

The incident wave itself has nonzero expansion coefficients for basis functions with the same parallel wave vector, and is straightforward to expand:  $|e_i|^2 = 2k_z k \delta_{p, p'} |E_0|^2$ , where  $p'$  is the incident polarization,  $E_0$  is the plane wave amplitude, and  $k = |\mathbf{k}|$ . The optimal polarization currents only comprise waves with parallel wave vector identical to that of the incident wave, simplifying the final bounds. Normalizing the bounds of Eqs. (14)–(16) by the  $z$ -directed plane-wave intensity,  $|E_0|^2 k_z / 2k$ , gives cross-sections bounds for extended structures:

$$\sigma_{\text{ext}}/A \leq 2 \sum_{s=\pm} \frac{\rho_{s, p'}}{\text{Im} \xi + \rho_{s, p'}} \quad (18)$$

$$\sigma_{\text{abs}}/A \leq \frac{(\nu^*)^2}{2} \sum_{s=\pm} \frac{\rho_{s, p'}}{(\nu^* - 1) \text{Im} \xi + \nu^* \rho_{s, p'}} \quad (19)$$

$$\sigma_{\text{sca}}/A \leq \frac{(\nu^*)^2}{2} \sum_{s=\pm} \frac{\rho_{s, p'}}{\nu^* \text{Im} \xi + (\nu^* - 1) \rho_{s, p'}}, \quad (20)$$

where  $A$  is the total surface area and  $\rho_{s, p'}$  denotes the radiation loss by a scattering channel with parity  $s$ , polarization  $p'$ , and parallel wave vector  $\mathbf{k}_\parallel$ . Again, the use of a high-symmetry bounding volume results in analytical expressions that are easy to compute.

Figure 3(a) compares the upper bounds for the normalized cross-sections with the cross-sections of silver thin

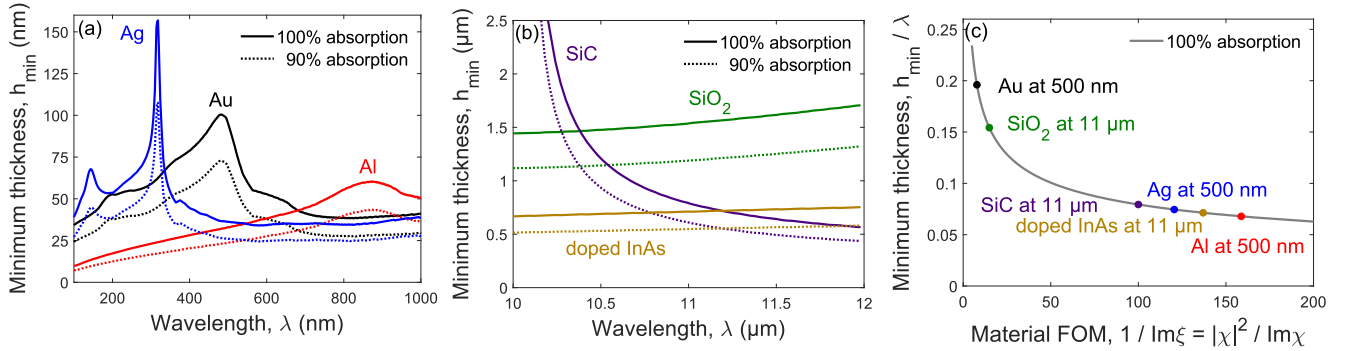


FIG. 4. Minimum thickness required for a perfect absorber to reach 90% and 100% absorption rate under normal incidence for typical materials that are polaritonic at (a) visible [64] and (b) infrared wavelengths [65–67]. (c) A universal curve showing minimum thickness for 100% absorption, on which all perfect-absorber materials can be judged by their material FOM,  $1/\text{Im}\xi = |\chi|^2/\text{Im}\chi$ .

films at normal incidence and wavelength  $\lambda = 800\text{ nm}$ . Here we choose the longer wavelength due to its potential for an ultra-thin perfect absorber, discussed below. In Figs. 3(b,c) we explore whether it is possible to approach the derived bounds. We use inverse design [68–75], a large-scale computational optimization technique for discovering optimal configurations of many design parameters, to design patterned Drude-metal films that approach their bounds. We denote the Drude metal plasma frequency by  $\omega_p$  and plasma wavelength by  $\lambda_p = 2\pi c/\omega_p$ . Figure 3(b) depicts the bounds (red solid line) and the performance of thin films (black solid line) as a function of thickness, as well as six different inverse-design structures that bridge most of the gap from the thin films to the bounds. The incident wavelength is  $2.78\lambda_p$  and the period is  $0.25\lambda_p$ , with minimum feature size  $0.025\lambda_p$ . For an ultrathin absorber with thickness  $h = 0.1\lambda_p$ , the inverse-designed metasurface can reach 82% of the global bound. In Fig. 3(c) we isolate the design at the smallest thickness (triangle marker in Fig. 3(b)) and show its spectral absorption percentage, as well as its geometrical design (inset). We impose a constraint of binary material distribution (given pointwise in the SM), but we do not impose lithographic or other fabrication constraints since the objective is to compare against the global bounds. It is apparent that inverse design can come rather close to the bounds, suggesting they may be “tight” or nearly so.

An important ramification of the bounds of Eqs. (18)–(20) is that they can be used to find the minimum thickness of any patterned “perfect absorber” [76–78], achieving 100% absorption or close to it. Such absorbers are particularly useful for sensing applications [77, 79]. Absorption cross-section per area,  $\sigma_{\text{abs}}/A$ , is the percentage absorption, while the bound on the right-hand side of Eq. (19) is a function only of the incident angle, the absorber thickness (defined as the thickness of its minimum bounding film), and its material susceptibility  $\chi(\omega)$ . For normally incident waves, we show in the SM that the minimum thickness  $h_{\min}$  to achieve 100% absorption is

given by the self-consistent equation

$$h_{\min} = \left( \frac{2\lambda}{\pi} \right) \frac{\text{Im}\xi}{1 - \text{sinc}^2(kh_{\min})}. \quad (21)$$

Figure 4(a,b) shows the minimum thicknesses (solid lines) for 100% absorption in common metallic and polar-dielectric materials. It is perhaps surprising how large the thicknesses are, averaging on the order of 50 nm for metals [64] at visible wavelengths and 1  $\mu\text{m}$  for polar dielectrics [65–67] at infrared wavelengths. The only previous bounds that could predict a minimal thickness for perfect absorption are the material-loss bounds [7], which predict minimal thicknesses on the order of 0.5 nm and 10 nm for the same materials and wavelengths, respectively. Also included in the figures are the minimal thicknesses for 90% absorption, which are close to the 100%-absorption curves. In the SM, we present further analysis suggesting two points: first, that the minimum thickness is typically larger than the skin depth, and can be arbitrarily larger; second, that the nearly linear dependence of Aluminum’s minimal thickness relative to wavelength indicates Drude-like permittivity, in contrast to highly non-Drude-like behavior for Ag and Au. In Fig. 4(c) we present a universal curve on which all perfect-absorber materials can be judged, showing the minimum thickness relative to the wavelength as a function of the inverse of material loss,  $1/\text{Im}\xi = |\chi|^2/\text{Im}\chi$ , which is a material “figure of merit” (FOM) as discussed above [7]. As material losses become increasingly small (and  $1/\text{Im}\xi$  increasingly large), there are diminishing returns to further reductions in loss; in the SM we show that in the far subwavelength limit,  $h_{\min} \ll \lambda$ , the minimum thickness scales with material FOM as  $h_{\min}/\lambda \sim (1/\text{Im}\xi)^{-1/3}$ .

#### IV. THERMAL ABSORPTION AND EMISSION

Our formalism applies equally to thermal absorption and emission. By Kirchhoff’s Law (reciprocity), or its

nonreciprocal generalization [80], total thermal absorption and emission are equivalent and can be found by considering a weighted average of incoherent, orthogonal incoming fields  $\mathbf{E}_{\text{inc},i}$ :

$$\langle |\mathbf{E}_{\text{inc}}|^2 \rangle = \sum_i w_i |\mathbf{E}_{\text{inc},i}|^2, \quad (22)$$

where  $w_i$  is a weighting factor. For a continuum of incoming fields the sum is instead an integral with a differential weight. A direct consequence of the incoherent averaging is that an upper bound to the average absorptivity/emissivity is given by the average of the bounds for each independent incident field. Surprisingly, the bounds computed by this averaging procedure varies depending on which basis is used for the incoming fields. If the incident field is treated as an incoherent sum of plane waves, over all propagation angles, for example, then the absorptivity/emissivity cross-section bounds would simply be a scalar multiple of Eq. (15). However, the bound can be tightened (decreased) if the incident fields are instead decomposed in vector spherical waves, for which the weight function  $w_i$  is determined by the fluctuation-dissipation theorem [81]:  $w_i = \frac{4}{\pi\omega}\Theta(T)$ , where  $\Theta(T) = \hbar\omega/(e^{\hbar\omega/k_B T} - 1)$  is the Planck energy of a harmonic oscillator at temperature  $T$  without the zero-point energy. The resulting bound, derived in the SM, is a sum over all VSW channels  $i$ :

$$P_{\text{abs}} \leq \frac{2}{\pi}\Theta(T) \sum_i \begin{cases} \frac{\rho_i \text{Im} \xi}{(\text{Im} \xi + \rho_i)^2} & \text{for } \rho_i \leq \text{Im} \xi \\ \frac{1}{4} & \text{for } \rho_i \geq \text{Im} \xi \end{cases} \quad (23)$$

where  $i = \{n, m, j\}$  includes all VSW channels:  $n = 1, 2, \dots$ ,  $m = -n, \dots, n$ ,  $j = 1, 2$ , and the sum converges for any nonzero  $\text{Im} \xi$ . Eq. (23) shows a distinct threshold behavior within each VSW channel. In the asymptotic limits of radiation-dominant ( $\rho_i \gg \text{Im} \xi$ ) or material-loss-dominant ( $\rho_i \ll \text{Im} \xi$ ) scenarios, Eq. (23) simplifies to the known channel- [10] and material-loss bounds [7]. In tandem, accounting for both mechanisms yields a significantly tighter bound than any previous approach.

Taking the same approach as in Sec. III, the bound for any arbitrary shape is no larger than the bound for any bounding volume of that shape, and thus we can compute analytical bounds for finite-sized thermal absorbers with spherical bounding volumes. Figure 5 shows the thermal absorption/emission cross-section as a function of the size of a spherical silver [63] nanoparticle at wavelength  $\lambda = 360 \text{ nm}$ . Included is the bound of Eq. (23), which is nearly achieved by the sphere at its ideal resonant size. We also include the recently published  $\mathbb{T}$ -operator bound of Ref. [40], which considered the effect of radiation and material losses separately for thermal sources. As shown in Fig. 5, by incorporating both losses in one optical theorem constraint, even for thermal fields the new bounds are slightly tighter.

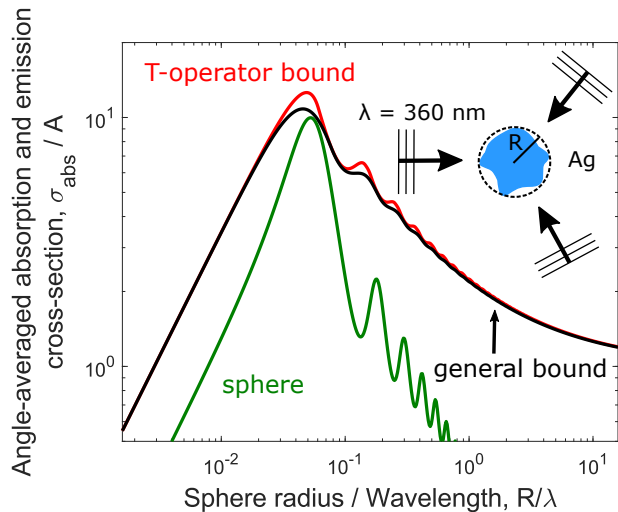


FIG. 5. General bound for maximum thermal absorption and emission, compared with  $\mathbb{T}$ -operator bound and thermal absorption of an actual Ag [63] sphere with radius  $R$ .

## V. DISCUSSION AND EXTENSIONS

In this Article, we have shown that an energy-conservation law, arising as a generalized optical theorem, enables identification of maximal electromagnetic response at a single frequency. We considered: arbitrary linear and quadratic response functions, Eq. (6), power-flow quantities such as absorption and scattering, Eqs. (8,9), and LDOS, Eqs. (10)–(12), and more specific scenarios such as plane-wave scattering, Eqs. (14)–(21), and thermal absorption/emission, Eq. (23). In this section, we briefly touch on numerous other applications where this formalism can be seamlessly applied.

A natural extension of this work is to the emergent field of 2D materials [82–86]. From a theoretical perspective the only difference with a 2D material is that the induced polarization currents exist on a two-dimensional surfaces instead of within a three-dimensional volume, which would change the interpretation of  $\phi$  in Eq. (4), and would change the domain of the Green's function  $\Gamma_0$ , but otherwise the remainder of the derivation is identical. Instead of rederiving the bounds in a 2D domain, however, a simpler approach is to substitute the bulk susceptibility  $\chi$  by the expression  $\chi \rightarrow i\sigma_{2D}/\omega h$ , where  $\sigma_{2D}$  is the 2D-material conductivity and  $h$  is an infinitesimal thickness going to zero. (The bounds do not diverge because the geometric or bounding volume is also proportional to  $h$ , canceling the  $1/h$  divergence in the material parameter.) Then, all of the bounds derived herein apply to 2D materials as well.

Another important extension is to problems of field concentration *away* from the scatterer itself. In surface-enhanced Raman scattering [87–89], for example, where recently material-loss bounds have been derived [17], it is important to maximize average field enhancement over



a plane close to but not overlapping the scatterer itself. In this case the objective might be the integral of the scattered-field intensity over a plane  $P$ , i.e.  $\int_P \psi_{\text{scat}}^\dagger \psi_{\text{scat}}$ . The scattering field is the convolution of the background Green's function with the polarization fields  $\phi$ , such that this objective is a quadratic function of the polarization fields:  $\phi^\dagger \left[ \int_P \Gamma_0^\dagger \Gamma_0 \right] \phi$ , which is exactly of the form required by Eq. (4) and thus is bounded above by Eq. (6).

Similarly, cross density of states [90] measures the coupling strength between dipoles at two spatial locations, typically coupled via near-field interactions, for applications including Förster energy transfer [91] and quantum entanglement [92]. Such coupling effectively reduces to optimizing the field strength at one location from a point source at another location, mapping identically to the field concentration problem.

Maximizing optical forces and torques has been a topic of substantial interest [14, 29–32], and is one that our framework applies to very naturally. One can compute force and torque via surface integrals of quantities related to the Maxwell stress tensor, which is a quadratic function of the electric and magnetic fields. By the same connection of the scattered fields to the induced polarization fields, it is possible to write any force/torque optimization function as a sum of quadratic- and linear-in-polarization terms, thereby equivalent to Eq. (4) and subject to the bounds of Eq. (6).

During the preparation of this manuscript, a preprint appeared [93] that contains similar ideas to those contained here. It is recognized in Ref. [93] that one can utilize the equality of absorption plus scattering and extinction, i.e. Eq. (3), as a quadratic electromagnetic constraint. They further show that an additional constraint can be identified; essentially, the real-part analog of Eq. (3). In this context they provide bounds very similar to ours for power-flow quantities and local density of states, they consider the problem of directional scattering, and they show a two-parameter dual formulation for incorporating the second constraint. Conversely, they do not have bounds for arbitrary linear and quadratic

functions, i.e. our Eq. (6), or for non-scalar or nonlocal susceptibility operators, nor do they consider the applications of perfect absorption or thermal absorption and emission. And they do not identify the optimal value of the dual variable  $\nu^*$ , which is important, for example, in determining the analytical bounds of Eqs. (21,23). Without an analytical value for  $\nu^*$ , it is not possible to identify the minimum thickness of a perfect absorber.

Looking forward, the energy-conservation approach developed here provides a framework for further generalizations and unifications. The incorporation of multiple constraints naturally leads to connections to the optimization field of semidefinite programming [94], as utilized in Ref. [95], where rapid global-optimization computational techniques are well-established [96]. Away from single-frequency problems, the question of how to incorporate nonzero bandwidth in a bound framework would have important ramifications. As shown in Ref. [19], it may be possible to do so through generalized quadratic constraints based on causality. Finally, a key variable missing from conservation-law-based approaches to bounds is the refractive index of a transparent medium, which appears in bounds pertaining to the broadband absorption of sunlight [97–100], but otherwise do not appear in any of the bounds referenced here. Accounting for refractive index may require a unification of conservation-law approaches with, perhaps, those based on Lagrangian duality [101]. With such generalizations and unifications, it may be possible to understand the extreme limits of electromagnetic response in any scenario.

## VI. ACKNOWLEDGMENTS

Z.K. and L.Z. were supported by the Army Research Office under grant number W911NF-19-1-0279. O.D.M. was partially supported by the Army Research Office under grant number W911NF-19-1-0279 and partially supported by the Air Force Office of Scientific Research under award number FA9550-17-1-0093.

- 
- [1] A. D. Yaghjian, Sampling criteria for resonant antennas and scatterers, *J. Appl. Phys.* **79**, 7474 (1996).
  - [2] R. E. Hamam, A. Karalis, J. Joannopoulos, and M. Soljačić, Coupled-mode theory for general free-space resonant scattering of waves, *Physical review A* **75**, 053801 (2007).
  - [3] D.-H. Kwon and D. M. Pozar, Optimal characteristics of an arbitrary receive antenna, *IEEE Transactions on Antennas and Propagation* **57**, 3720 (2009).
  - [4] Z. Ruan and S. Fan, Design of subwavelength superscattering nanospheres, *Applied Physics Letters* **98**, 043101 (2011).
  - [5] I. Liberal, Y. Ra'di, R. Gonzalo, I. Ederra, S. A. Tretyakov, and R. W. Ziolkowski, Least upper bounds of the powers extracted and scattered by bi-anisotropic particles, *IEEE Transactions on Antennas and Propagation* **62**, 4726 (2014).
  - [6] I. Liberal, I. Ederra, R. Gonzalo, and R. W. Ziolkowski, Upper bounds on scattering processes and metamaterial-inspired structures that reach them, *IEEE Transactions on Antennas and Propagation* **62**, 6344 (2014).
  - [7] O. D. Miller, A. G. Polimeridis, M. H. Reid, C. W. Hsu, B. G. DeLacy, J. D. Joannopoulos, M. Soljačić, and S. G. Johnson, Fundamental limits to optical response in absorptive systems, *Optics express* **24**, 3329 (2016).
  - [8] O. D. Miller, O. Ilic, T. Christensen, M. H. Reid, H. A. Atwater, J. D. Joannopoulos, M. Soljačić, and S. G. Johnson, Limits to the optical response of graphene and two-dimensional materials, *Nano letters* **17**, 5408

- (2017).
- [9] Y. Yang, O. D. Miller, T. Christensen, J. D. Joannopoulos, and M. Soljacic, Low-loss plasmonic dielectric nanoresonators, *Nano letters* **17**, 3238 (2017).
  - [10] J. Pendry, Radiative exchange of heat between nanostructures, *Journal of Physics: Condensed Matter* **11**, 6621 (1999).
  - [11] S. Thongrattanasiri, F. H. L. Koppens, and F. J. García de Abajo, Complete optical absorption in periodically patterned graphene, *Physical Review Letters* **108**, 10.1103/PhysRevLett.108.047401 (2012).
  - [12] J.-P. Hugonin, M. Besbes, and P. Ben-Abdallah, Fundamental limits for light absorption and scattering induced by cooperative electromagnetic interactions, *Physical Review B* **91**, 180202 (2015).
  - [13] O. D. Miller, S. G. Johnson, and A. W. Rodriguez, Shape-independent limits to near-field radiative heat transfer, *Physical review letters* **115**, 204302 (2015).
  - [14] A. Rahimzadegan, R. Alaei, I. Fernandez-Corbaton, and C. Rockstuhl, Fundamental limits of optical force and torque, *Physical Review B* **95**, 035106 (2017).
  - [15] Y. Liu, L. Fan, Y. E. Lee, N. X. Fang, S. G. Johnson, and O. D. Miller, Optimal nanoparticle forces, torques, and illumination fields, *ACS Photonics* **6**, 395 (2018).
  - [16] Y. Yang, A. Massuda, C. Roques-Carnes, S. E. Kooi, T. Christensen, S. G. Johnson, J. D. Joannopoulos, O. D. Miller, I. Kaminer, and M. Soljačić, Maximal spontaneous photon emission and energy loss from free electrons, *Nature Physics* **14**, 894 (2018).
  - [17] J. Michon, M. Benzouia, W. Yao, O. D. Miller, and S. G. Johnson, Limits to surface-enhanced raman scattering near arbitrary-shape scatterers, *Optics Express* **27**, 35189 (2019).
  - [18] S. Nordebo, G. Kristensson, M. Mirmoosa, and S. Tret'yakov, Optimal plasmonic multipole resonances of a sphere in lossy media, *Physical Review B* **99**, 054301 (2019).
  - [19] H. Shim, L. Fan, S. G. Johnson, and O. D. Miller, Fundamental limits to near-field optical response over any bandwidth, *Physical Review X* **9**, 011043 (2019).
  - [20] Y. Ivanenko, M. Gustafsson, and S. Nordebo, Optical theorems and physical bounds on absorption in lossy media, *Optics Express* **27**, 34323 (2019).
  - [21] E. J. C. Dias and F. J. García de Abajo, Fundamental limits to the coupling between light and 2d polaritons by small scatterers, *ACS Nano* **13**, 5184 (2019).
  - [22] J. D. Jackson, Classical electrodynamics (1999).
  - [23] R. G. Newton, Optical theorem and beyond, *American Journal of Physics* **44**, 639 (1976).
  - [24] C. F. Bohren and D. R. Huffman, *Absorption and scattering of light by small particles* (John Wiley & Sons, 2008).
  - [25] P. S. Carney, J. C. Schotland, and E. Wolf, Generalized optical theorem for reflection, transmission, and extinction of power for scalar fields, *Physical Review E* **70**, 036611 (2004).
  - [26] D. Polder and M. Van Hove, Theory of Radiative Heat Transfer between Closely Spaced Bodies, *Phys. Rev. B* **4**, 3303 (1971).
  - [27] C. R. Otey, L. Zhu, S. Sandhu, and S. Fan, Fluctuational electrodynamics calculations of near-field heat transfer in non-planar geometries: A brief overview, *J. Quant. Spectrosc. Radiat. Transf.* **132**, 3 (2014).
  - [28] A. W. Rodriguez, M. T. H. Reid, and S. G. Johnson, Fluctuating-surface-current formulation of radiative heat transfer for arbitrary geometries, *Phys. Rev. B* **86**, 220302 (2012).
  - [29] M. Mazilu, J. Baumgartl, S. Kosmeier, and K. Dhoklakia, Optical Eigenmodes; exploiting the quadratic nature of the light-matter interaction, *Opt. Express* **19**, 933 (2011).
  - [30] Y. E. Lee, O. D. Miller, M. T. H. Reid, S. G. Johnson, and N. X. Fang, Computational inverse design of non-intuitive illumination patterns to maximize optical force or torque, *Opt. Express* **25**, 6757 (2017).
  - [31] Y. Liu, L. Fan, Y. E. Lee, N. X. Fang, S. G. Johnson, and O. D. Miller, Optimal nanoparticle forces, torques, and illumination fields, *ACS Photonics* **6**, 395 (2019).
  - [32] M. Horodyski, M. Kühmayer, A. Brandstötter, K. Pichler, Y. V. Fyodorov, U. Kuhl, and S. Rotter, Optimal wave fields for micromanipulation in complex scattering environments, *Nat. Photonics* **10**, 1038/s41566-019-0550-z (2019).
  - [33] D. A. B. Miller, Waves, modes, communications, and optics: a tutorial, *Adv. Opt. Photonics* **11**, 679 (2019).
  - [34] R. G. Newton, *Scattering theory of waves and particles* (Springer Science & Business Media, 2013).
  - [35] C. Mahaux and H. A. Weidenmüller, Shell-model approach to nuclear reactions., *Soft Matter* (1969).
  - [36] D. Jalas, A. Petrov, M. Eich, W. Freude, S. Fan, Z. Yu, R. Baets, M. Popović, A. Melloni, J. D. Joannopoulos, *et al.*, What is—and what is not—an optical isolator, *Nature Photonics* **7**, 579 (2013).
  - [37] S. Rotter and S. Gigan, Light fields in complex media: Mesoscopic scattering meets wave control, *Reviews of Modern Physics* **89**, 015005 (2017).
  - [38] W. L. Stutzman and G. A. Thiele, *Antenna theory and design*, 3rd ed. (John Wiley & Sons, 2012).
  - [39] R. Loudon, *The Quantum Theory of Light*, 3rd ed. (Oxford University Press, New York, 2000).
  - [40] S. Molesky, W. Jin, P. S. Venkataram, and A. W. Rodriguez, T operator bounds on angle-integrated absorption and thermal radiation for arbitrary objects, *Physical Review Letters* **123**, 257401 (2019).
  - [41] S. Molesky, P. S. Venkataram, W. Jin, and A. W. Rodriguez, Fundamental limits to radiative heat transfer: theory, *arXiv preprint arXiv:1907.03000* (2019).
  - [42] P. S. Venkataram, S. Molesky, P. Chao, and A. W. Rodriguez, Fundamental limits to attractive and repulsive casimir–polder forces, *arXiv preprint arXiv:1911.10295* (2019).
  - [43] W. C. Chew, *Waves and fields in inhomogeneous media* (IEEE press, 1995).
  - [44] Y. Yang, D. Zhu, W. Yan, A. Agarwal, M. Zheng, J. D. Joannopoulos, P. Lalanne, T. Christensen, K. K. Berggren, and M. Soljačić, A general theoretical and experimental framework for nanoscale electromagnetism, *Nature* **576**, 248 (2019).
  - [45] A. Fallahi, T. Low, M. Tamagnone, and J. Perruisseau-Carrier, Nonlocal electromagnetic response of graphene nanostructures, *Phys. Rev. B* **91**, 121405(R) (2015).
  - [46] A. G. Polimeridis, M. H. Reid, S. G. Johnson, J. K. White, and A. W. Rodriguez, On the computation of power in volume integral equation formulations, *IEEE Transactions on Antennas and Propagation* **63**, 611 (2014).

- [47] J. A. Kong, Theorems of bianisotropic media, *Proceedings of the IEEE* **60**, 1036 (1972).
- [48] E. M. Purcell and C. R. Pennypacker, Scattering and Absorption of Light by Nonspherical Dielectric Grains, *Astrophys. J.* **186**, 705 (1973).
- [49] M. T. H. Reid, O. D. Miller, A. G. Polimeridis, A. W. Rodriguez, E. M. Tomlinson, and S. G. Johnson, Photon torpedoes and rytov pinwheels: Integral-equation modeling of non-equilibrium fluctuation-induced forces and torques on nanoparticles, arXiv:1708.01985 (2017).
- [50] A. Welters, Y. Avniel, and S. G. Johnson, Speed-of-light limitations in passive linear media, *Physical Review A* **90**, 023847 (2014).
- [51] A. Ben-Tal and M. Teboulle, Hidden convexity in some nonconvex quadratically constrained quadratic programming, *Mathematical Programming* **72**, 51 (1996).
- [52] S. Boyd and L. Vandenberghe, *Convex optimization* (Cambridge university press, 2004).
- [53] L. Novotny and B. Hecht, *Principles of nano-optics* (Cambridge university press, 2012).
- [54] X. Liang and S. G. Johnson, Formulation for scalable optimization of microcavities via the frequency-averaged local density of states, *Optics express* **21**, 30812 (2013).
- [55] E. M. Purcell, H. C. Torrey, and R. V. Pound, Resonance absorption by nuclear magnetic moments in a solid, *Physical review* **69**, 37 (1946).
- [56] A. Taflove, A. Oskooi, and S. G. Johnson, *Advances in FDTD computational electrodynamics: photonics and nanotechnology* (Artech house, 2013) Chap. 4, pp. 65–100.
- [57] Y. Xu, R. K. Lee, and A. Yariv, Quantum analysis and the classical analysis of spontaneous emission in a microcavity, *Physical Review A* **61**, 033807 (2000).
- [58] F. Wijnands, J. Pendry, F. Garcia-Vidal, P. Bell, P. Roberts, L. Marti, *et al.*, Green's functions for maxwell's equations: application to spontaneous emission, *Optical and Quantum Electronics* **29**, 199 (1997).
- [59] O. J. Martin and N. B. Piller, Electromagnetic scattering in polarizable backgrounds, *Physical Review E* **58**, 3909 (1998).
- [60] G. D'Aguanno, N. Mattiucci, M. Centini, M. Scalora, and M. J. Bloemer, Electromagnetic density of modes for a finite-size three-dimensional structure, *Physical Review E* **69**, 057601 (2004).
- [61] K. Joulain, R. Carminati, J.-P. Mulet, and J.-J. Greffet, Definition and measurement of the local density of electromagnetic states close to an interface, *Physical Review B* **68**, 245405 (2003).
- [62] K. Joulain, J.-P. Mulet, F. Marquier, R. Carminati, and J.-J. Greffet, Surface electromagnetic waves thermally excited: Radiative heat transfer, coherence properties and casimir forces revisited in the near field, *Surface Science Reports* **57**, 59 (2005).
- [63] P. B. Johnson and R.-W. Christy, Optical constants of the noble metals, *Physical review B* **6**, 4370 (1972).
- [64] E. D. Palik, *Handbook of optical constants of solids*, Vol. 3 (Academic press, 1998).
- [65] S. Law, L. Yu, A. Rosenberg, and D. Wasserman, All-semiconductor plasmonic nanoantennas for infrared sensing, *Nano letters* **13**, 4569 (2013).
- [66] M. Francoeur, M. P. Mengüç, and R. Vaillon, Spectral tuning of near-field radiative heat flux between two thin silicon carbide films, *Journal of Physics D: Applied Physics* **43**, 075501 (2010).
- [67] S. Popova, T. Tolstykh, and V. Vorobev, Optical characteristics of amorphous quartz in the 1400-200 cm<sup>-1</sup> region, *Opt. Spectrosc* **33**, 444 (1972).
- [68] A. Jameson, L. Martinelli, and N. A. Pierce, Optimum Aerodynamic Design Using the Navier-Stokes Equations, *Theor. Comput. Fluid Dyn.* **10**, 213 (1998).
- [69] O. Sigmund and J. Søndergaard Jensen, Systematic design of phononic band-gap materials and structures by topology optimization, *Philos. Trans. R. Soc. London. Ser. A Math. Phys. Eng. Sci.* **361**, 1001 (2003).
- [70] J. Lu, S. Boyd, and J. Vucković, Inverse design of a three-dimensional nanophotonic resonator, *Opt. Express* **19**, 10563 (2011).
- [71] J. S. Jensen and O. Sigmund, Topology optimization for nano-photonics, *Laser & Photonics Rev.* **5**, 308 (2011).
- [72] O. D. Miller, *Photonic Design: From Fundamental Solar Cell Physics to Computational Inverse Design*, Ph.D. thesis, University of California, Berkeley (2012).
- [73] C. M. Lalau-Keraly, S. Bhargava, O. D. Miller, and E. Yablonovitch, Adjoint shape optimization applied to electromagnetic design, *Optics Express* **21**, 21693 (2013).
- [74] V. Ganapati, O. D. Miller, and E. Yablonovitch, Light trapping textures designed by electromagnetic optimization for subwavelength thick solar cells, *IEEE Journal of Photovoltaics* **4**, 175 (2014).
- [75] N. Aage, E. Andreassen, B. S. Lazarov, and O. Sigmund, Giga-voxel computational morphogenesis for structural design, *Nature* **550**, 84 (2017).
- [76] C. M. Watts, X. Liu, and W. J. Padilla, Metamaterial electromagnetic wave absorbers, *Adv. Mater.* **24**, 10.1002/adma.201200674 (2012).
- [77] Y. P. Lee, J. Y. Rhee, Y. J. Yoo, and K. W. Kim, *Metamaterials for perfect absorption*, Vol. 236 (Springer, 2016).
- [78] N. Landy, S. Sajuyigbe, J. Mock, D. Smith, and W. Padilla, Perfect Metamaterial Absorber, *Phys. Rev. Lett.* **100**, 207402 (2008).
- [79] N. Liu, M. Mesch, T. Weiss, M. Hentschel, and H. Giessen, Infrared perfect absorber and its application as plasmonic sensor, *Nano Lett.* **10**, 2342 (2010).
- [80] D. A. Miller, L. Zhu, and S. Fan, Universal modal radiation laws for all thermal emitters, *Proc. Natl. Acad. Sci. U. S. A.* **114**, 4336 (2017).
- [81] M. Krüger, G. Bimonte, T. Emig, and M. Kardar, Trace formulas for nonequilibrium casimir interactions, heat radiation, and heat transfer for arbitrary objects, *Physical Review B* **86**, 115423 (2012).
- [82] K. S. Novoselov, D. Jiang, F. Schedin, T. J. Booth, V. V. Khotkevich, S. V. Morozov, and A. K. Geim, Two-dimensional atomic crystals, *Proc. Natl. Acad. Sci.* **102**, 10451 (2005).
- [83] A. K. Geim and K. Novoselov, The rise of graphene, *Nat. Mater.* **6**, 183 (2007).
- [84] F. H. L. Koppens, D. E. Chang, and F. J. G. D. Abajo, Graphene Plasmonics: A Platform for Strong Light-Matter Interactions, *Nano Lett.* **11**, 3370 (2011).
- [85] D. N. Basov, M. M. Fogler, and F. J. Garcia de Abajo, Polaritons in van der Waals materials, *Science* **354**, aag1992 (2016).
- [86] T. Low, A. Chaves, J. D. Caldwell, A. Kumar, N. X. Fang, P. Avouris, T. F. Heinz, F. Guinea, L. Martin-Moreno, and F. Koppens, Polaritons in layered two-

- dimensional materials, *Nat. Mater.* **16**, 182 (2016).
- [87] M. Moskovits, Surface-enhanced spectroscopy, *Rev. Mod. Phys.* **57**, 783 (1985).
  - [88] S. Nie and S. R. Emory, Probing single molecules and single nanoparticles by surface-enhanced Raman scattering, *Science* **275**, 1102 (1997).
  - [89] P. L. Stiles, J. A. Dieringer, N. C. Shah, and R. P. Van Duyne, Surface-Enhanced Raman Spectroscopy, *Annu. Rev. Anal. Chem.* **1**, 601 (2008).
  - [90] A. Cazé, R. Pierrat, and R. Carminati, Spatial coherence in complex photonic and plasmonic systems, *Physical Review Letters* **110**, 063903 (2013).
  - [91] J. A. Gonzaga-Galeana and J. R. Zurita-Sánchez, A re-visitation of the Förster energy transfer near a metallic spherical nanoparticle: (1) efficiency enhancement or reduction? (2) the control of the Förster radius of the unbounded medium. (3) the impact of the local density of states, *The Journal of Chemical Physics* **139**, 244302 (2013).
  - [92] A. Gonzalez-Tudela, D. Martin-Cano, E. Moreno, L. Martin-Moreno, C. Tejedor, and F. J. Garcia-Vidal, Entanglement of two qubits mediated by one-dimensional plasmonic waveguides, *Physical Review Letters* **106**, 020501 (2011).
  - [93] M. Gustafsson, K. Schab, L. Jelinek, and M. Capek, Upper bounds on absorption and scattering, *arXiv preprint arXiv:1912.06699* (2019).
  - [94] Z. Q. Luo, W. K. Ma, A. So, Y. Ye, and S. Zhang, Semidefinite relaxation of quadratic optimization problems, *IEEE Signal Processing Magazine* **27**, 20 (2010).
  - [95] H. Shim, H. Chung, and O. D. Miller, Maximal free-space concentration of electromagnetic waves, *arXiv:1905.10500* (2019).
  - [96] J. Nocedal and S. J. Wright, *Numerical Optimization*, 2nd ed. (Springer, New York, NY, 2006).
  - [97] E. Yablonovitch, Statistical ray optics, *J. Opt. Soc. Am.* **72**, 899 (1982).
  - [98] Z. Yu, A. Raman, and S. Fan, Fundamental limit of nanophotonic light trapping in solar cells, *Proc. Natl. Acad. Sci. U. S. A.* **107**, 17491 (2010).
  - [99] S. Buddhiraju and S. Fan, Theory of solar cell light trapping through a nonequilibrium Green's function formulation of Maxwell's equations, *Phys. Rev. B* **96**, 1 (2017).
  - [100] M. Benzaouia, G. Tokic, O. D. Miller, D. K. P. Yue, and S. G. Johnson, From solar cells to ocean buoys: Wide-bandwidth limits to absorption by metaparticle arrays, *Physical Review Applied* **11**, 034033 (2019).
  - [101] G. Angeris, J. Vuckovic, and S. P. Boyd, Computational Bounds for Photonic Design, *ACS Photonics* **6**, 1232 (2019).



# Supplementary Material: Maximal single-frequency electromagnetic response

Zeyu Kuang,<sup>1</sup> Lang Zhang,<sup>1</sup> and Owen D. Miller<sup>1</sup>

<sup>1</sup>*Department of Applied Physics and Energy Sciences Institute,  
Yale University, New Haven, Connecticut 06511, USA*

(Dated: December 21, 2024)

## CONTENTS

I. The optimization problem and its dual function	1
II. Absorbed, scattered, and extinguished power expressions	3
III. Bound for a nonmagnetic scalar material under plane wave incidence	4
IV. General bound for extended scatterers	5
V. Minimum thickness for perfect absorbers	5
VI. Inverse-designed ultrathin absorber	6
VII. Deriving previous bounds from general bound formalism	7
VIII. Eigenvalues of $\text{Im } \mathbb{G}_0^{\text{EE}}$ for a sphere	8
IX. Eigenvalues of $\text{Im } \mathbb{G}_0^{\text{EE}}$ for a film	9
X. Upper bounds at different generality	10
XI. Bound for local density of states (LDOS)	12
References	16

## I. THE OPTIMIZATION PROBLEM AND ITS DUAL FUNCTION

The optimization problem is to maximize a response function  $f(\phi) = \phi^\dagger \mathbb{A} \phi + \text{Im} [\beta^\dagger \phi]$  under the optical theorem constraint, where the variable  $\phi$  is polarization current induced in the scatterer. Parameter  $\beta$  is any vector, and  $\mathbb{A}$  is any self-adjoint operator. Following the standard optimization notation, we rewrite it as a minimization problem by adding a minus sign to the objective function:

$$\begin{aligned} \min_{\phi} \quad & -f(\phi) = -\phi^\dagger \mathbb{A} \phi - \text{Im} [\beta^\dagger \phi] \\ \text{s.t.} \quad & \phi^\dagger \{\text{Im } \xi + \text{Im } \Gamma_0\} \phi = \text{Im} [\psi_{\text{inc}}^\dagger \phi]. \end{aligned} \quad (1)$$

Operator  $\text{Im } \Gamma_0$  is positive semidefinite, representing radiative loss of the system. Operator  $\text{Im } \xi$  is positive definite, representing material loss of the system. The optimization problem stated in Eq. (1) is known to have strong duality [1], prompting us to find its dual function, which in turn is defined by its Lagrangian:

$$L(\phi, \nu) = \phi^\dagger \mathbb{B}(\nu) \phi - \text{Im} [(\beta + \nu \psi_{\text{inc}})^\dagger \phi], \quad (2)$$

where we introduce dual variable  $\nu$  and simplify our notation by introducing operator

$$\mathbb{B}(\nu) = -\mathbb{A} + \nu(\text{Im } \xi + \text{Im } \Gamma_0). \quad (3)$$

The dual function  $g(\nu)$  is defined as the minimum of Lagrangian  $L(\phi, \nu)$  over variable  $\phi$ . We denote  $\nu_0$  as the value of  $\nu$  when the minimum eigenvalue of  $\mathbb{B}(\nu)$  is zero, leaving  $\mathbb{B}(\nu_0)$  a positive semidefinite operator with at least one

zero eigenvalue. For  $\nu < \nu_0$ , the positivity of  $\text{Im } \xi + \text{Im } \Gamma_0$  implies that  $\mathbb{B}(\nu) = \mathbb{B}(\nu_0) - (\nu_0 - \nu)(\text{Im } \xi + \text{Im } \Gamma_0)$  has negative eigenvalues and  $L(\phi, \nu)$  is unbounded below. For  $\nu > \nu_0$ ,  $\mathbb{B}(\nu) = \mathbb{B}(\nu_0) + (\nu - \nu_0)(\text{Im } \xi + \text{Im } \Gamma_0)$  is positive definite, and  $L(\phi, \nu)$  is convex in  $\phi$  with a finite minimal value. This minimum is obtained at

$$\phi(\nu) = \frac{i}{2} \mathbb{B}^{-1}(\nu)(\beta + \nu \psi_{\text{inc}}), \quad (4)$$

with the resulting dual function:

$$g(\nu) = \min_{\phi} L(\phi, \nu) = \begin{cases} -\frac{1}{4}(\beta + \nu \psi_{\text{inc}})^{\dagger} \mathbb{B}^{-1}(\nu)(\beta + \nu \psi_{\text{inc}}) & \nu > \nu_0 \\ -\infty & \nu < \nu_0. \end{cases} \quad (5)$$

Lastly, at  $\nu = \nu_0$ , if  $\beta + \nu_0 \psi_{\text{inc}}$  is in the range of  $\mathbb{B}(\nu_0)$ , then  $L(\phi, \nu)$  is still convex and  $g(\nu_0)$  takes the value of the first case in Eq. (5) with the inverse operator replaced by the pseudo-inverse; if not, then Eq. (2) suggests that  $L(\phi, \nu)$  is unbounded below and  $g(\nu_0) \rightarrow -\infty$ .

Due to strong duality, the optimization problem, Eq. (1), is solved by finding the maximum of the dual function:

$$\max_{\nu} g(\nu), \quad (6)$$

According to Eq. (5), dual function  $g(\nu)$  is maximized at a value within range  $[\nu_0, +\infty)$ , which we denote as  $\nu^*$ . The maximum response function takes the (negative of the optimal dual) value:

$$f_{\text{max}} = \frac{1}{4}(\beta + \nu^* \psi_{\text{inc}})^{\dagger} \mathbb{B}^{-1}(\nu^*)(\beta + \nu^* \psi_{\text{inc}}), \quad (7)$$

and the optimal polarization current  $\phi$  is given by evaluating Eq. (4) at  $\nu^*$ :

$$\phi^* = \frac{i}{2} \mathbb{B}^{-1}(\nu^*)(\beta + \nu^* \psi_{\text{inc}}), \quad (8)$$

except when  $\nu^* = \nu_0$ , where the  $\phi^*$  can not be uniquely determined due to the presence of zero eigenvalues in  $\mathbb{B}(\nu_0)$ .

To solve for the maximum response function  $f_{\text{max}}$  in Eq. (7), we need to find the optimal dual variable  $\nu^*$ , which can only occur either in the interior of the domain  $[\nu_0, \infty)$  or its boundary. If  $\nu^*$  is in the interior, it has to satisfy the condition:

$$\left. \frac{\partial g(\nu)}{\partial \nu} \right|_{\nu=\nu^*} = 0. \quad (9)$$

This can be translated to a transcendental equation that determines the first possible optimum which we denote as  $\nu_1$ :

$$2\psi_{\text{inc}}^{\dagger} \mathbb{B}^{-1}(\nu_1)(\beta + \nu_1 \psi_{\text{inc}}) - (\beta + \nu_1 \psi_{\text{inc}})^{\dagger} \mathbb{B}^{-1}(\nu_1) \mathbb{B}'(\nu_1) \mathbb{B}^{-1}(\nu_1)(\beta + \nu_1 \psi_{\text{inc}}) = 0. \quad (10)$$

A dual function is concave [1]; hence, if  $\nu_1$  exists in the domain  $(\nu_0, \infty)$  then it must be the global optimizer of  $g(\nu)$ . If not, then there is no point in the domain at which the gradient is zero, and  $\nu^*$  must be one of the boundary values of  $[\nu_0, \infty)$ ; by the concavity of  $g(\nu)$ , the maximum must occur at  $\nu_0$ . Hence we have:

$$\nu^* = \begin{cases} \nu_1 & \text{if } \nu_1 \in (\nu_0, \infty) \\ \nu_0 & \text{else.} \end{cases} \quad (11)$$

The self-consistency implicit in Eq. (10) for  $\nu_1$  can make it difficult to ascertain whether  $\nu_1$  or  $\nu_0$  is optimal. Instead, if the derivative of  $g(\nu)$  at  $\nu_0$  is well-defined, we can check its value to determine whether  $g(\nu)$  attains its extremum in the interior of its domain or on its boundary: if and only if it is positive, then  $\nu_1$  will be in the interior of the domain  $[\nu_0, \infty)$ . Hence, if  $\beta + \nu_0 \psi_{\text{inc}}$  is in the range of  $\mathbb{B}^{-1}(\nu_0)$ , then we can also use the equivalent condition to determine  $\nu^*$ :

$$\nu^* = \begin{cases} \nu_1 & \text{if } 2\psi_{\text{inc}}^{\dagger} \mathbb{B}^{-1}(\nu_0)(\beta + \nu_0 \psi_{\text{inc}}) < (\beta + \nu_0 \psi_{\text{inc}})^{\dagger} \mathbb{B}^{-1}(\nu_0) \mathbb{B}'(\nu_0) \mathbb{B}^{-1}(\nu_0)(\beta + \nu_0 \psi_{\text{inc}}) \\ \nu_0 & \text{else.} \end{cases} \quad (12)$$

## II. ABSORBED, SCATTERED, AND EXTINGUISHED POWER EXPRESSIONS

We start with extinguished power which is linear in polarization current  $\phi$ :  $P_{\text{ext}} = \frac{\omega}{2} \text{Im} [\psi_{\text{inc}}^\dagger \phi]$ . For simplicity, we take the objective function as  $\text{Im} [\psi_{\text{inc}}^\dagger \phi]$ , and set  $\mathbb{A} = 0$  and  $\beta = \psi_{\text{inc}}$  in the optimization problem, Eq. (1). The operator defined in Eq. (3) becomes  $\mathbb{B}(\nu) = \nu(\text{Im} \xi + \text{Im} \Gamma_0)$ . Its minimum eigenvalue reaches zero when  $\nu = \nu_0 = 0$ . Dual function in Eq. (5) takes the form:

$$g(\nu) = \begin{cases} -\frac{(\nu+1)^2}{4} \psi_{\text{inc}}^\dagger (\text{Im} \xi + \text{Im} \Gamma_0)^{-1} \psi_{\text{inc}} & \nu > 0 \\ -\infty & \nu \leq 0, \end{cases} \quad (13)$$

where we identified  $g(\nu_0) = -\infty$  since  $\beta + \nu_0 \psi_{\text{inc}}$  is not in the range of  $B(\nu_0)$ . Since  $g(\nu_0) = -\infty$ , the optimal dual variable  $\nu^*$  can only be chosen at  $\nu_1$ . Solving Eq. (10) gives  $\nu_1 = 1$  and the maximum extinction given by Eq. (7) is (after adding back the  $\frac{\omega}{2}$  prefactor):

$$P_{\text{ext}}^{\text{max}} = \frac{\omega}{2} \psi_{\text{inc}}^\dagger (\text{Im} \xi + \text{Im} \Gamma_0)^{-1} \psi_{\text{inc}}. \quad (14)$$

The optimum polarization current  $\phi^*$  is given by Eq. (8):

$$\phi^* = i(\text{Im} \xi + \text{Im} \Gamma_0)^{-1} \psi_{\text{inc}}. \quad (15)$$

Absorption has the form  $P_{\text{abs}} = \frac{\omega}{2} \phi^\dagger (\text{Im} \xi) \phi$ . Taking the objective function as  $\phi^\dagger (\text{Im} \xi) \phi$ , we have  $\mathbb{A} = \text{Im} \xi$  and  $\beta = 0$  in the optimization problem, Eq. (1). The operator defined in Eq. (3) becomes  $\mathbb{B}(\nu) = (\nu - 1) \text{Im} \xi + \nu \text{Im} \Gamma_0$ . Dual function takes the form of Eq. (5):

$$g(\nu) = \begin{cases} -\frac{\nu^2}{4} \psi_{\text{inc}}^\dagger [(\nu - 1) \text{Im} \xi + \nu \text{Im} \Gamma_0]^{-1} \psi_{\text{inc}} & \nu > \nu_0 \\ -\infty & \nu < \nu_0, \end{cases} \quad (16)$$

At  $\nu = \nu_0$ , the value of  $g(\nu_0) \rightarrow -\infty$  if  $\psi_{\text{inc}}$  is not in the range of  $\mathbb{B}(\nu_0)$ , otherwise  $g(\nu_0)$  takes the form of the first case in Eq. (16) with the inverse replaced by pseudo-inverse. As in Eq. (11), the optimal dual variable  $\nu^*$  is obtained either at the interval  $(\nu_0, \infty)$  or its boundary  $\nu_0$ . The value of  $\nu_0$  depends on the nature of both  $\text{Im} \xi$  and  $\text{Im} \Gamma_0$ . The value of  $\nu_1$  is given by Eq. (10):

$$\psi_{\text{inc}}^\dagger [2\mathbb{B}^{-1}(\nu_1) - \nu_1 \mathbb{B}^{-1}(\nu_1)(\text{Im} \xi + \text{Im} \Gamma_0)\mathbb{B}^{-1}(\nu_1)] \psi_{\text{inc}} = 0. \quad (17)$$

Using Eq. (7) and adding back the  $\frac{\omega}{2}$  prefactor, we have maximum absorption:

$$P_{\text{abs}}^{\text{max}} = \frac{\omega}{2} \frac{\nu^{*2}}{4} \psi_{\text{inc}}^\dagger [(\nu^* - 1) \text{Im} \xi + \nu^* \text{Im} \Gamma_0]^{-1} \psi_{\text{inc}}. \quad (18)$$

The optimal current can be determined by Eq. (8) in the case of  $\nu^* = \nu_1$ :

$$\phi^* = i \frac{\nu^*}{2} [(\nu^* - 1) \text{Im} \xi + \nu^* \text{Im} \Gamma_0]^{-1} \psi_{\text{inc}}. \quad (19)$$

Scattering power has the form  $P_{\text{scat}} = \frac{\omega}{2} \phi^\dagger (\text{Im} \Gamma_0) \phi$ , such that  $\mathbb{A} = \text{Im} \Gamma_0$  and  $\beta = 0$  after suppressing the  $\frac{\omega}{2}$  prefactor. Following a similar procedure as absorption, we have maximum scattering as:

$$P_{\text{scat}}^{\text{max}} = \frac{\omega}{2} \frac{\nu^{*2}}{4} \psi_{\text{inc}}^\dagger [(\nu^* - 1) \text{Im} \xi + \nu^* \text{Im} \Gamma_0]^{-1} \psi_{\text{inc}}. \quad (20)$$

Again,  $\nu^*$  takes two possible values:  $\nu_1$  and  $\nu_0$ , as dictated by Eq. (11). The determinant equation for  $\nu_1$  takes the same form as Eq. (17) with  $\mathbb{B}(\nu) = \nu \text{Im} \xi + (\nu - 1) \text{Im} \Gamma_0$ .

An equivalent formulation for all three power quantities is to write them as the difference (or sum) of the other two. For example, scattering power can be written as the difference between extinction and absorption:  $P_{\text{scat}} = \frac{\omega}{2} \text{Im} [\psi_{\text{inc}}^\dagger \phi] - \frac{\omega}{2} \phi^\dagger (\text{Im} \xi) \phi$ . With  $\mathbb{A} = -\text{Im} \xi$  and  $\beta = \psi_{\text{inc}}$  after suppressing the  $\frac{\omega}{2}$  prefactor, this gives the same optima as in Eq. (20) but with a different form:

$$P_{\text{scat}}^{\text{max}} = \frac{\omega}{2} \frac{(1 + \nu^*)^2}{4} \psi_{\text{inc}}^\dagger [(\nu^* + 1) \text{Im} \xi + \nu^* \text{Im} \Gamma_0]^{-1} \psi_{\text{inc}}, \quad (21)$$

where the optimal dual variable  $\nu^*$  is determined by Eq. (11).

### III. BOUND FOR A NONMAGNETIC SCALAR MATERIAL UNDER PLANE WAVE INCIDENCE

Let us consider a typical case where the incident field is a plane wave and the scatterer is composed of nonmagnetic scalar material. Here, we only need to consider the electric response in Eq. (14, 18, 20), so we can replace  $\psi_{\text{inc}}$  with  $\mathbf{e}_{\text{inc}}$ ,  $\Gamma_0$  with  $\mathbb{G}_0^{\text{EE}}$ , and  $\xi = \text{Im } \chi / |\chi|^2$  is now a scalar with  $\chi$  being the electric susceptibility of the material. Because  $\text{Im } \mathbb{G}_0^{\text{EE}}$  is positive-semidefinite, we can simplify its eigendecomposition to write  $\text{Im } \mathbb{G}_0^{\text{EE}} = \mathbb{V} \mathbb{V}^\dagger$ , where the columns of  $\mathbb{V}$ , which we denote  $\mathbf{v}_i$ , form an orthogonal basis of polarization currents. They are normalized such that the set  $\rho_i = \mathbf{v}_i^\dagger \mathbf{v}_i$  are the eigenvalues of  $\text{Im } \mathbb{G}_0^{\text{EE}}$  and represent the powers radiated by unit-normalization polarization currents. The expansion of incident plane wave,  $\mathbf{e}_{\text{inc}}$ , in these channels is assumed to be:  $\mathbf{e}_{\text{inc}} = \frac{1}{k^{3/2}} \sum_i e_i \mathbf{v}_i$ , where the exact value of  $|e_i|^2$  depends on the choice of  $\mathbf{v}_i$ . Throughout the SM, we use uncapitalized symbol  $\mathbf{e}_{\text{inc}}$  to denote the incident electric field to emphasis its vector nature.

We decompose general bounds given by Eq. (14, 18, 20) into contributions from these channels:

$$P_{\text{ext}} \leq \frac{\omega}{2} \frac{1}{k^3} \sum_i |e_i|^2 \frac{\rho_i}{\text{Im } \xi + \rho_i} \quad (22)$$

$$P_{\text{abs}} \leq \frac{\omega}{2} \frac{\nu^{*2}}{4} \frac{1}{k^3} \sum_i |e_i|^2 \frac{\rho_i}{(\nu^* - 1) \text{Im } \xi + \nu^* \rho_i} \quad (23)$$

$$P_{\text{scat}} \leq \frac{\omega}{2} \frac{\nu^{*2}}{4} \frac{1}{k^3} \sum_i |e_i|^2 \frac{\rho_i}{\nu^* \text{Im } \xi + (\nu^* - 1) \rho_i}. \quad (24)$$

Taking  $\omega = k$  in our unitless convention and write  $k = 2\pi/\lambda$  gives the expressions presented in the main text. Bounds for both absorption and scattering contain  $\nu^*$ , which is determined by Eq. (11). For absorption,  $\nu_0 = 1$ , and  $\nu_1$  is computationally evaluated by solving the following equation:

$$\sum_i |e_i|^2 \frac{(\nu_1 - 2) \text{Im } \xi + \nu_1 \rho_i}{[(\nu_1 - 1) \text{Im } \xi + \nu_1 \rho_i]^2} = 0. \quad (25)$$

For scattering bound,  $\nu_0 = \rho_{\text{max}}/(\rho_{\text{max}} + \text{Im } \xi)$ , where  $\rho_{\text{max}}$  is the largest  $\rho_i$ . The other potential optimum,  $\nu_1$ , can be determined from Eq. (25) with the role of  $\text{Im } \xi$  and  $\rho_i$  interchanged.

Bounds on maximal cross sections for a finite-size scatterer is obtained by normalizing Eqs. (22)–(24) by plane wave intensity  $|E_0|^2/2$  (the vacuum resistance  $Z_0 = 1$ ):

$$\sigma_{\text{ext}} \leq \frac{\lambda^2}{4\pi^2 |E_0|^2} \sum_i |e_i|^2 \frac{\rho_i}{\text{Im } \xi + \rho_i} \quad (26)$$

$$\sigma_{\text{abs}} \leq \frac{\lambda^2}{4\pi^2 |E_0|^2} \frac{\nu^{*2}}{4} \sum_i |e_i|^2 \frac{\rho_i}{(\nu^* - 1) \text{Im } \xi + \nu^* \rho_i} \quad (27)$$

$$\sigma_{\text{scat}} \leq \frac{\lambda^2}{4\pi^2 |E_0|^2} \frac{\nu^{*2}}{4} \sum_i |e_i|^2 \frac{\rho_i}{\nu^* \text{Im } \xi + (\nu^* - 1) \rho_i}. \quad (28)$$

For a plane wave incidence with  $|e_i|^2 = \pi(2n+1)\delta_{m,\pm 1}|E_0|^2$ , we can simplify the above expression by summing over index  $m, j$  within  $i = \{m, n, j\}$ , leaving contributions indexed only by total angular momentum  $n$ :

$$\sigma_{\text{ext}} \leq \frac{\lambda^2}{\pi} \sum_n (2n+1) \frac{\rho_i}{\text{Im } \xi + \rho_i} \quad (29)$$

$$\sigma_{\text{abs}} \leq \frac{\lambda^2}{\pi} \frac{\nu^{*2}}{4} \sum_n (2n+1) \frac{\rho_i}{(\nu^* - 1) \text{Im } \xi + \nu^* \rho_i} \quad (30)$$

$$\sigma_{\text{scat}} \leq \frac{\lambda^2}{\pi} \frac{\nu^{*2}}{4} \sum_n (2n+1) \frac{\rho_i}{\nu^* \text{Im } \xi + (\nu^* - 1) \rho_i}. \quad (31)$$

In Fig. 2(c) of the main text, we use the notation  $\sigma_{\text{ext},n}$  to denote the contribution from the  $n$ -th channel in the summation of Eq. (29).



#### IV. GENERAL BOUND FOR EXTENDED SCATTERERS

We assume the material is isotropic, nonmagnetic, and homogeneous so the extended scatterer only has electric response to the incident field. The most general far-field incidence has the expansion in its electric field:

$$\mathbf{e}_{\text{inc}} = \frac{1}{k^{3/2}} \sum_i \int_{k_{\parallel} \leq k} e_i(\mathbf{k}_{\parallel}) \mathbf{v}_i(\mathbf{k}_{\parallel}) \frac{d\mathbf{k}_{\parallel}}{(2\pi)^2}, \quad (32)$$

where index  $i = \{s, p\}$ . Plugging the expansion of  $\mathbf{e}_{\text{inc}}$  in Eq. (14, 18, 20) gives the integral form of cross-sections bounds after normalization by the z-directed plane wave intensity  $|E_0|^2 k_z / 2k$ :

$$\sigma_{\text{ext}} \leq \frac{1}{k k_z |E_0|^2} \sum_i \int_{k_{\parallel} \leq k} |e_i(\mathbf{k}_{\parallel})|^2 \frac{\rho_i(\mathbf{k}_{\parallel})}{\text{Im} \xi + \rho_i(\mathbf{k}_{\parallel})} \frac{d\mathbf{k}_{\parallel}}{(2\pi)^2} \quad (33)$$

$$\sigma_{\text{abs}} \leq \frac{1}{k k_z |E_0|^2} \frac{\nu^{*2}}{4} \sum_i \int_{k_{\parallel} \leq k} |e_i(\mathbf{k}_{\parallel})|^2 \frac{\rho_i(\mathbf{k}_{\parallel})}{(\nu^* - 1) \text{Im} \xi + \nu^* \rho_i(\mathbf{k}_{\parallel})} \frac{d\mathbf{k}_{\parallel}}{(2\pi)^2} \quad (34)$$

$$\sigma_{\text{scat}} \leq \frac{1}{k k_z |E_0|^2} \frac{\nu^{*2}}{4} \sum_i \int_{k_{\parallel} \leq k} |e_i(\mathbf{k}_{\parallel})|^2 \frac{\rho_i(\mathbf{k}_{\parallel})}{\nu^* \text{Im} \xi + (\nu^* - 1) \rho_i(\mathbf{k}_{\parallel})} \frac{d\mathbf{k}_{\parallel}}{(2\pi)^2}. \quad (35)$$

Now we restrict our scope to a plane wave incidence with total wave vector  $\mathbf{k} = k_x \hat{\mathbf{e}}_x + k_y \hat{\mathbf{e}}_y + k_z \hat{\mathbf{e}}_z$  and polarization  $p'$ . We denote its parallel wave vector as  $\mathbf{k}'_{\parallel} = k_x \hat{\mathbf{e}}_x + k_y \hat{\mathbf{e}}_y$  where the  $'$  symbol differentiates  $\mathbf{k}'_{\parallel}$  from  $\mathbf{k}_{\parallel}$  that is used to label different channels in Eq. (32). The plane wave has the expression:

$$\mathbf{e}_{\text{inc}} = E_0 \hat{\mathbf{e}} e^{i\mathbf{k}'_{\parallel} \cdot \mathbf{r}_{\parallel}} e^{ik_z z}, \quad (36)$$

where  $\hat{\mathbf{e}}$  is a unit vector denotes incident polarization, taking the form  $(k_y \hat{\mathbf{e}}_x - k_x \hat{\mathbf{e}}_y) / k'_{\parallel}$  for  $p' = M$ , and  $(-k_z \hat{\mathbf{k}}'_{\parallel} + k'_{\parallel} \hat{\mathbf{e}}_z) / k$  for  $p' = N$ . Equating Eq. (36) with Eq. (32) gives the expansion coefficients,  $e_i(\mathbf{k}_{\parallel})$ . Plugging its absolute value  $|e_i(\mathbf{k}_{\parallel})| = |E_0| \sqrt{2k_z k} (2\pi)^2 \delta(\mathbf{k}'_{\parallel} - \mathbf{k}_{\parallel}) \delta_{p,p'}$  into Eqs. (33)–(35) gives bounds for plane wave incidence:

$$\sigma_{\text{ext}} / A \leq 2 \sum_{s=\pm} \frac{\rho_{s,p'}(\mathbf{k}'_{\parallel})}{\text{Im} \xi + \rho_{s,p'}(\mathbf{k}'_{\parallel})} \quad (37)$$

$$\sigma_{\text{abs}} / A \leq \frac{\nu^{*2}}{2} \sum_{s=\pm} \frac{\rho_{s,p'}(\mathbf{k}'_{\parallel})}{(\nu^* - 1) \text{Im} \xi + \nu^* \rho_{s,p'}(\mathbf{k}'_{\parallel})} \quad (38)$$

$$\sigma_{\text{scat}} / A \leq \frac{\nu^{*2}}{2} \sum_{s=\pm} \frac{\rho_{s,p'}(\mathbf{k}'_{\parallel})}{\nu^* \text{Im} \xi + (\nu^* - 1) \rho_{s,p'}(\mathbf{k}'_{\parallel})}, \quad (39)$$

where we identified factor  $A = (2\pi)^2 \delta^2(0)$  corresponding to total surface area.

Bounds for both absorption and scattering contain  $\nu^*$ , which is determined by Eq. (11). For absorption,  $\nu_0 = 1$ , and  $\nu_1$  is computationally evaluated by solving the following equation:

$$\sum_{s=\pm} \frac{(\nu_1 - 2) \text{Im} \xi + \nu_1 \rho_{s,p'}(\mathbf{k}'_{\parallel})}{[(\nu_1 - 1) \text{Im} \xi + \nu_1 \rho_{s,p'}(\mathbf{k}'_{\parallel})]^2} = 0. \quad (40)$$

For scattering,  $\nu_0 = \rho_{\text{max}} / (\rho_{\text{max}} + \text{Im} \xi)$ , where  $\rho_{\text{max}}$  is the largest  $\rho_i$ . The other potential optimum,  $\nu_1$ , is determined by Eq. (40) with the role of  $\text{Im} \xi$  and  $\rho_i$  interchanged.

#### V. MINIMUM THICKNESS FOR PERFECT ABSORBERS

Following Section IV in the SM, this section studies minimum thickness required for a perfect absorber that has 100% absorption. Usually, one determines the optimal  $\nu^*$  in Eq. (38) by comparing the values of  $\nu_0$  and  $\nu_1$ . Here, we take an alternative approach introduced through Eq. (12), where the derivative of the dual function at  $\nu_0$  is used as a threshold, giving an explicit expression for maximum absorption cross section:

$$\sigma_{\text{abs}} / A \leq \begin{cases} \frac{\nu_1^2}{2} \sum_{s=\pm} \frac{\rho_{s,p'}(\mathbf{k}'_{\parallel})}{(\nu_1 - 1) \text{Im} \xi + \nu_1 \rho_{s,p'}(\mathbf{k}'_{\parallel})}, & \frac{1}{\text{Im} \xi} > \frac{1}{2} \left[ \frac{1}{\rho_{+,p'}(\mathbf{k}_{\parallel})} + \frac{1}{\rho_{-,p'}(\mathbf{k}_{\parallel})} \right] \\ 1. & \frac{1}{\text{Im} \xi} \leq \frac{1}{2} \left[ \frac{1}{\rho_{+,p'}(\mathbf{k}_{\parallel})} + \frac{1}{\rho_{-,p'}(\mathbf{k}_{\parallel})} \right] \end{cases} \quad (41)$$

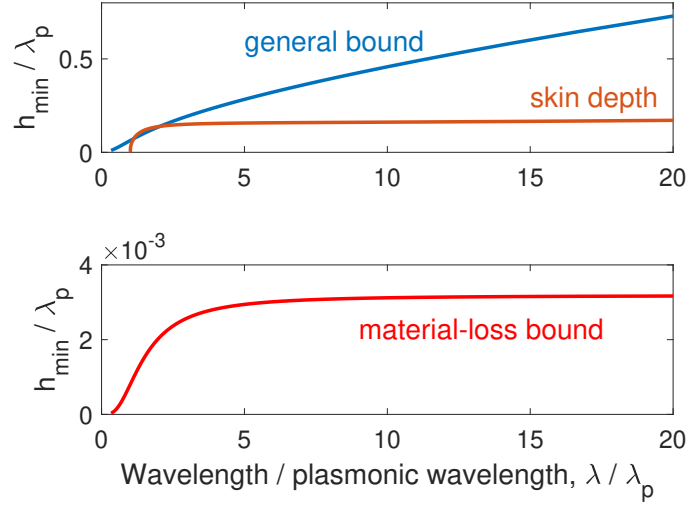


FIG. 1. Comparison between skin depth and minimum thickness,  $h_{\min}$ , for a perfect absorber as a function of wavelength  $\lambda$  for a Drude metal. General bound and material-loss bound are shown separately in two plots. The former one gives a much more modest prediction. All quantities are normalized by the plasmonic wavelength,  $\lambda_p$ , of the Drude metal.

Threshold for maximum absorption (at a given incident angle) corresponds to the condition:

$$\frac{1}{\text{Im } \xi} = \frac{1}{2} \left[ \frac{1}{\rho_{+,p'}(\mathbf{k}_{\parallel})} + \frac{1}{\rho_{-,p'}(\mathbf{k}_{\parallel})} \right], \quad (42)$$

where we can solve for its required minimum thickness:

$$h_{\min} = \frac{k_z}{k^2} \frac{4 \text{Im } \xi}{1 - \text{sinc}^2(k_z h_{\min})}. \quad (43)$$

Under normal incidence ( $k_z = k$ ), when the absorber is much thinner than the wavelength,  $kh_{\min} \rightarrow 0$ , it can be shown that:

$$kh_{\min} = (24 \text{Im } \xi)^{1/3}. \quad (44)$$

This predicts a much more modest improvement over reduced material loss, compared with previous material-loss bound [2] where the expression for minimum thickness under normal incidence is  $kh_{\min} = \text{Im } \xi$ . Fig. 1 shows that this contrast is on the order of  $10^2$  for a Drude metal modeled by permittivity

$$\varepsilon(\omega) = -\frac{\omega_p^2}{\omega^2 + i\gamma\omega}, \quad (45)$$

with loss rate  $\gamma = 0.02\omega_p$ . Plasmonic wavelength is  $\lambda_p = 2\pi c/\omega_p$ , with  $c = 1$  being the speed of light in our unitless convention.

It is also shown in Fig. 1 that, minimum thickness predicted by the general bound is on the same length scale as skin depth in the metal [3] near plasmonic wavelength,  $\lambda_p$ . For  $\lambda < \lambda_p$ , there is no surface plasmonic mode inside a Drude metal and skin depth is ill-defined, though it is still possible to realize a perfect absorber according to the general bound. For  $\lambda > \lambda_p$ , while both skin depth and material-loss bound reach a plateau at large wavelength limit, general bound has  $h_{\min}$  increases proportionally to wavelength. This comes from the effectively thinner material under large wavelength incidence and explains the behavior of Al in Fig. 4(a) of the main text.

## VI. INVERSE-DESIGNED ULTRATHIN ABSORBER

Absorption cross section bound given by Eq. (38) can be reached by an inverse-designed ultra-thin absorber within a factor of 2. This optimized structure has translational symmetry along y direction, with varying permittivity in x-z

$z/\lambda_p$	$x/\lambda_p$											
	-0.106	-0.087	-0.067	-0.048	-0.029	-0.010	0.010	0.029	0.048	0.067	0.087	0.106
0.0375	1	1	0	1	0	0	0	0	1	0	1	1
0.0125	1	1	1	1	1	0	0	1	1	1	1	1
-0.0125	1	1	1	1	0	0	0	0	1	1	1	1
-0.0375	1	1	1	1	0	0	0	0	1	1	1	1

TABLE I. Permittivity distribution of the inverse-designed ultrathin absorber in x-z plane, where 1 stands for Drude metal and 0 stands for air. Plane wave with wavelength  $\lambda = 2.78\lambda_p$  incidents from negative z-direction.

plane. The binary permittivity distribution is recorded in Table I with 0 denotes air and 1 denotes the material. Incident plane wave propagates in negative z direction. The material is modeled by a Drude metal:

$$\varepsilon(\omega) = 1 - \frac{\omega_p^2}{\omega^2 + i\omega\gamma}, \quad (46)$$

where  $\omega_p$  is its plasmonic frequency and  $\gamma = 0.1\omega_p$  is its damping rate. Its plasmonic wavelength is  $\lambda_p = 2\pi c/\omega_p$ .

## VII. DERIVING PREVIOUS BOUNDS FROM GENERAL BOUND FORMALISM

Different derivations of upper bounds can be formulated as optimization problems with same objective functions but different constraints. In this section, we showed that how the general bound, developed in this paper, can incorporate previous bounds by either relaxing the energy equality constraint, or taking the result of the general bound in certain limit.

	Extinction	Absorption	Scattering
General bound	$\max P_{\text{ext}}$ s.t. $P_{\text{scat}} + P_{\text{abs}} = P_{\text{ext}}$	$\max P_{\text{abs}}$ s.t. $P_{\text{scat}} + P_{\text{abs}} = P_{\text{ext}}$	$\max P_{\text{scat}}$ s.t. $P_{\text{scat}} + P_{\text{abs}} = P_{\text{ext}}$
Material bound [2]	$\max P_{\text{ext}}$ s.t. $P_{\text{abs}} \leq P_{\text{ext}}$	$\max P_{\text{abs}}$ s.t. $P_{\text{abs}} \leq P_{\text{ext}}$	$\max P_{\text{ext}} - P_{\text{abs}}$
Channel bound [4]	$\max P_{\text{ext}}$ s.t. $P_{\text{scat}} \leq P_{\text{ext}}$	$\max P_{\text{ext}} - P_{\text{scat}}$	$\max P_{\text{scat}}$ s.t. $P_{\text{scat}} \leq P_{\text{ext}}$

TABLE II. Upper bounds as optimization problems with the same objective function but different constraints. General bound uses an equality energy constraint, while the other two relax it to inequality constraints (or even unconstrained), resulting looser bounds.

	Extinction	Absorption	Scattering
General bound	$\psi_{\text{inc}}^\dagger (\text{Im } \xi + \text{Im } \Gamma_0)^{-1} \psi_{\text{inc}}$	$\frac{\nu^{*2}}{4} \psi_{\text{inc}}^\dagger [(\nu^* - 1) \text{Im } \xi + \nu^* \text{Im } \Gamma_0]^{-1} \psi_{\text{inc}}$	$\frac{\nu^{*2}}{4} \psi_{\text{inc}}^\dagger [(\nu^* - 1) \text{Im } \xi + \nu^* \text{Im } \Gamma_0]^{-1} \psi_{\text{inc}}$
Material bound [2]	$\psi_{\text{inc}}^\dagger (\text{Im } \xi)^{-1} \psi_{\text{inc}}$	$\psi_{\text{inc}}^\dagger (\text{Im } \xi)^{-1} \psi_{\text{inc}}$	$\frac{1}{4} \psi_{\text{inc}}^\dagger (\text{Im } \xi)^{-1} \psi_{\text{inc}}$
Channel bound [4]	$\psi_{\text{inc}}^\dagger (\text{Im } \Gamma_0)^{-1} \psi_{\text{inc}}$	$\frac{1}{4} \psi_{\text{inc}}^\dagger (\text{Im } \Gamma_0)^{-1} \psi_{\text{inc}}$	$\psi_{\text{inc}}^\dagger (\text{Im } \Gamma_0)^{-1} \psi_{\text{inc}}$

TABLE III. Optimum of different upper-bound formulations presented in Table II. Optimal dual variable of the general bound is determined by Eq. (11).

*a. channel and material loss bounds* Table II compares general bound with material-loss bound (material bound) and channel bound. General bound purposed in this paper utilizes the *equality* energy conservation constraint:  $P_{\text{scat}} + P_{\text{abs}} = P_{\text{ext}}$ . Throwing away either  $P_{\text{scat}}$  or  $P_{\text{abs}}$  gives the *inequality* energy conservation constraint used in previous material bound [2] or channel bound [4]. In both formalisms, the disregarded term itself is treated by an unconstrained optimization.

All optimization problems in Table II have strong duality, thus their optimums can be analytically determined by the optimal of their dual functions, given in Table III (with prefactor  $\omega/2$  suppressed in every expression). Results for material bound appears in [2]. Results for channel bound appears in [4]. Moreover, expanding channel bound into VSWs for a spherical scatterer gives the expressions in [5–8] (after adding back prefactor  $\omega/2$ ):  $P_{\text{scat}}^{\text{max}} = P_{\text{ext}}^{\text{max}} = 4P_{\text{abs}}^{\text{max}} = \frac{|E_0|^2}{k^2} \sum_{n=1}^{+\infty} \pi(2n+1)$ , where  $E_0$  is the plane wave amplitude,  $k$  is the amplitude of the wave vector, and  $n$  is total angular momentum.

*b. T-operator bound* As discussed in the main text, our bound is tighter than T-operator bound [9] for maximum absorption from a thermal incident field. Though using different approaches, the general bound can reproduce the same result as in T-operator bound by relaxing the energy constraint to  $P_{\text{abs}} \leq P_{\text{ext}}$  and replacing objective function  $P_{\text{abs}}$  with  $P_{\text{ext}} - P_{\text{scat}}$ :

$$\begin{aligned} \max \quad & P_{\text{ext}} - P_{\text{scat}} \\ \text{s.t.} \quad & P_{\text{abs}} \leq P_{\text{ext}}. \end{aligned} \quad (47)$$

Similar to Section I in the SM, we solve Eq. (47) by its dual function:

$$g(\lambda) = \frac{(\lambda+1)^2}{4} \psi_{\text{inc}}^\dagger [\text{Im } \Gamma_0 + \lambda \text{Im } \xi]^{-1} \psi_{\text{inc}}, \quad (48)$$

where  $\lambda$  is the notation used in [1] to denote dual variable for an inequality constraint. The range for  $\lambda$  is  $[0, +\infty)$ . When  $\lambda = 0$ , the inverse operator in Eq. (48) is ill-defined and we replace it with pseudo inverse if  $\psi_{\text{inc}} \in \text{Range}\{\text{Im } \Gamma_0\}$ , otherwise  $g(0) \rightarrow -\infty$ .

Following assumptions made in T-operator bound, we assume far-field thermal incidence and nonmagnetic material, where  $\psi_{\text{inc}}$  and  $\Gamma_0$  is replaced by  $\mathbf{e}_{\text{inc}}$  and  $\mathbb{G}_0^{\text{EE}}$ . As discussed in Section IV in the main text, thermal incident field can be expanded by a set of uncorrelated orthogonal fields. We choose it to be  $\{\mathbf{v}_i\}$ , the eigenvectors of  $\text{Im } \mathbb{G}_0^{\text{EE}}$ , with expansion coefficients given by  $|e_i|^2 = \frac{4}{\pi\omega} \Theta(T)$  and  $\Theta(T) = \hbar\omega / (e^{\hbar\omega/k_B T} - 1)$  is the Planck energy of a harmonic oscillator at temperature  $T$ .

Maximizing  $g(\lambda)$  gives the expression for optimal absorption of thermal incident fields in [9]:

$$P_{\text{abs}} \leq \frac{2}{\pi} \Theta(T) \sum_i \begin{cases} \frac{\rho_i}{\text{Im } \xi} & \text{for } 2\rho_i \leq \text{Im } \xi \\ \frac{1}{4} & \text{for } 2\rho_i \geq \text{Im } \xi, \end{cases} \quad (49)$$

where two cases correspond to optimal dual variable taking the value of either  $\nu_1 \in (0, +\infty)$  or  $\nu_0 = 0$ . Such a bound is looser than the general bound presented in Section IV of the main text, as a result of its inequality energy constraint in Eq. (47), rather than the equality energy constraint.

*c. patterned thin film bound* It is predicted that within a vacuum background, a patterned thin film with thickness much smaller than the incident wavelength has a maximum absorption of 50% [10]. To validate this, we take the limit  $k_z h \rightarrow 0$  in Eq. (41) and obtain:

$$\sigma_{\text{abs}}/A \leq \frac{2(\text{Im } \xi)\rho_{+,p'}}{(\text{Im } \xi + \rho_{+,p'})^2}. \quad (50)$$

Because a thin film only has dipole radiation that is symmetric respect to the  $z = 0$  plane, only mode with index  $s = +$  survived in Eq. (50).

When  $\text{Im } \xi = \rho_{+,M}$ , the absorption rate  $\sigma_{\text{abs}}/A$  in Eq. (50) reaches its maximum of 50%, agreeing with the prediction made in [10]. The advantage of our formalism is that we can also predict the minimum thickness for the patterned thin film to reach 50% absorption:  $h_{\text{min}} = 2 \text{Im } \xi / k$ , as solved from the optimal condition  $\text{Im } \xi = \rho_{+,M}$ .

### VIII. EIGENVALUES OF $\text{Im } \mathbb{G}_0^{\text{EE}}$ FOR A SPHERE

The expressions of  $\text{Im } \mathbb{G}_0^{\text{EE}}$  is given in [11], whose imaginary part is Hermitian and can be decomposed as:

$$\text{Im } \mathbb{G}_0^{\text{EE}} = \frac{1}{2i} (\mathbb{G}_0^{\text{EE}} - \mathbb{G}_0^{\text{EE}\dagger}) = \sum_{n,m,j} \mathbf{v}_{n,m,j} \mathbf{v}_{n,m,j}^\dagger, \quad (51)$$



where  $n = 1, 2, \dots$ ,  $m = -n, \dots, n$ ,  $j = 1, 2$  represents two polarizations.  $\mathbf{v}_{n,m,j}$  are regularized VSWs whose definition can be found in [11]:

$$\mathbf{v}_{n,m,1}(\mathbf{x}) = k^{\frac{3}{2}} Rg\mathbf{M}_{n,m}(kr, \theta, \phi) \quad (52)$$

$$\mathbf{v}_{n,m,2}(\mathbf{x}) = k^{\frac{3}{2}} Rg\mathbf{N}_{n,m}(kr, \theta, \phi). \quad (53)$$

The inner product of  $\mathbf{v}_{n,m,j}$  with itself gives the eigenvalue of  $\text{Im } \mathbb{G}_0^{\text{EE}}$ :

$$\rho_{n,m,j} = \mathbf{v}_{n,m,j}^\dagger \mathbf{v}_{n,m,j} \quad (54)$$

$$= \int_V \mathbf{v}_{n,m,j}^*(\mathbf{x}) \cdot \mathbf{v}_{n,m,j}(\mathbf{x}) dV. \quad (55)$$

Integrating over angular coordinates gives the expression:

$$\rho_{n,m,1} = \int_0^{kR} x^2 j_n^2(x) dx \quad (56)$$

$$\rho_{n,m,2} = n(n+1) \int_0^{kR} j_n^2(x) dx + \int_0^{kR} [x j_n(x)]'^2 dx, \quad (57)$$

which can be computationally evaluated or even reduced to simpler analytical forms [12].

## IX. EIGENVALUES OF $\text{Im } \mathbb{G}_0^{\text{EE}}$ FOR A FILM

As in [11, 13],  $\text{Im } \mathbb{G}_0^{\text{EE}}$  in Cartesian coordinate can be decomposed into a complete set of plane waves:

$$\text{Im } \mathbb{G}_0^{\text{EE}} = \sum_{s,p} \int_{k_{\parallel} \leq k} \mathbf{v}_{s,p}(\mathbf{k}_{\parallel}) \mathbf{v}_{s,p}^\dagger(\mathbf{k}_{\parallel}) \frac{d\mathbf{k}_{\parallel}}{(2\pi)^2}. \quad (58)$$

Index  $s = \{-1, +1\}$  represents odd and even parity, index  $p = M, N$  represents different polarization,  $\mathbf{k}_{\parallel}$  are in-plane wave vector whose integration only runs through propergating modes. Real-space expressions of  $\mathbf{v}_{s,p}(\mathbf{k}_{\parallel})$  are:

$$\mathbf{v}_{+,M}(\mathbf{k}_{\parallel}, \mathbf{x}) = ik \frac{e^{i\mathbf{k}_{\parallel} \cdot \mathbf{r}_{\parallel}}}{\sqrt{2k_z k_{\parallel}}} (k_y \hat{\mathbf{e}}_x - k_x \hat{\mathbf{e}}_y) \cos(k_z z) \quad (59)$$

$$\mathbf{v}_{-,M}(\mathbf{k}_{\parallel}, \mathbf{x}) = -ik \frac{e^{i\mathbf{k}_{\parallel} \cdot \mathbf{r}_{\parallel}}}{\sqrt{2k_z k_{\parallel}}} (k_y \hat{\mathbf{e}}_x - k_x \hat{\mathbf{e}}_y) \sin(k_z z) \quad (60)$$

$$\mathbf{v}_{+,N}(\mathbf{k}_{\parallel}, \mathbf{x}) = \frac{e^{i\mathbf{k}_{\parallel} \cdot \mathbf{r}_{\parallel}}}{\sqrt{2k_z}} \left[ k_{\parallel} \cos(k_z z) \hat{\mathbf{z}} - ik_z \sin(k_z z) \hat{\mathbf{k}}_{\parallel} \right] \quad (61)$$

$$\mathbf{v}_{-,N}(\mathbf{k}_{\parallel}, \mathbf{x}) = \frac{e^{i\mathbf{k}_{\parallel} \cdot \mathbf{r}_{\parallel}}}{\sqrt{2k_z}} \left[ k_{\parallel} \sin(k_z z) \hat{\mathbf{z}} + ik_z \cos(k_z z) \hat{\mathbf{k}}_{\parallel} \right]. \quad (62)$$

Inner products of  $\mathbf{v}_{s,p}(\mathbf{k}_{\parallel})$  in a thin film (thickness  $h$ , centered at  $z = 0$ ) is [9]:

$$\mathbf{v}_{s,p}^\dagger(\mathbf{k}_{\parallel}) \mathbf{v}_{s',p'}(\mathbf{k}'_{\parallel}) = \int_V \mathbf{v}_{s,p}^*(\mathbf{k}_{\parallel}, \mathbf{x}) \cdot \mathbf{v}_{s',p'}(\mathbf{k}'_{\parallel}, \mathbf{x}) dV \quad (63)$$

$$= \rho_{s,p}(\mathbf{k}_{\parallel}) (2\pi)^2 \delta(\mathbf{k}_{\parallel} - \mathbf{k}'_{\parallel}) \delta_{s,s'} \delta_{p,p'}, \quad (64)$$

where the eigenvalues are:

$$\rho_{\pm,M}(\mathbf{k}_{\parallel}) = \frac{k^2 h}{4k_z} \left( 1 \pm \frac{\sin(k_z h)}{k_z h} \right) \quad (65)$$

$$\rho_{\pm,N}(\mathbf{k}_{\parallel}) = \frac{k^2 h}{4k_z} \left( 1 \pm \frac{\sin(k_z h)}{k_z h} \right) \mp \frac{\sin(k_z h)}{2}. \quad (66)$$

## X. UPPER BOUNDS AT DIFFERENT GENERALITY

1. Most general form (include non-local, magnetic, inhomogeneous materials, any incident field, any geometry of the scatterer):

**Most general form:**  
**any material, shape, and incident field**

$$P_{\text{ext}} \leq \frac{\omega}{2} \psi_{\text{inc}}^\dagger (\text{Im } \xi + \text{Im } \Gamma_0)^{-1} \psi_{\text{inc}} \quad (67)$$

$$P_{\text{abs}} \leq \frac{\omega}{2} \frac{\nu^{*2}}{4} \psi_{\text{inc}}^\dagger [(\nu^* - 1) \text{Im } \xi + \nu^* \text{Im } \Gamma_0]^{-1} \psi_{\text{inc}} \quad (68)$$

$$P_{\text{scat}} \leq \frac{\omega}{2} \frac{\nu^{*2}}{4} \psi_{\text{inc}}^\dagger [\nu^* \text{Im } \xi + (\nu^* - 1) \text{Im } \Gamma_0]^{-1} \psi_{\text{inc}}, \quad (69)$$

where  $\text{Im } \xi$  and  $\text{Im } \Gamma_0$  are operators that depends on the exact shape and material compositions of the scatterer.

2. Scalar material (electric or magnetic scalar material, any incident field, any geometry of the homogeneous scatterer):

**Scalar material: any shape and incident field**

$$P_{\text{ext}} \leq \frac{\omega}{2} \frac{1}{\text{Im } \xi} \left[ \psi_{\text{inc}}^\dagger \psi_{\text{inc}} - \psi_{\text{inc}}^\dagger \mathbb{V} (\text{Im } \xi + \mathbb{V}^\dagger \mathbb{V})^{-1} \mathbb{V}^\dagger \psi_{\text{inc}} \right] \quad (70)$$

$$P_{\text{abs}} \leq \frac{\omega}{2} \frac{\nu^{*2}}{4} \frac{\nu^*}{\nu^* - 1} \frac{1}{\text{Im } \xi} \left\{ \frac{1}{\nu^*} \psi_{\text{inc}}^\dagger \psi_{\text{inc}} - \psi_{\text{inc}}^\dagger \mathbb{V} [(\nu^* - 1) \text{Im } \xi + \nu^* \mathbb{V}^\dagger \mathbb{V}]^{-1} \mathbb{V}^\dagger \psi_{\text{inc}} \right\} \quad (71)$$

$$P_{\text{scat}} \leq \frac{\omega}{2} \frac{\nu^{*2}}{4} \frac{\nu^* - 1}{\nu^*} \frac{1}{\text{Im } \xi} \left\{ \frac{1}{\nu^* - 1} \psi_{\text{inc}}^\dagger \psi_{\text{inc}} - \psi_{\text{inc}}^\dagger \mathbb{V} [\nu^* \text{Im } \xi + (\nu^* - 1) \mathbb{V}^\dagger \mathbb{V}]^{-1} \mathbb{V}^\dagger \psi_{\text{inc}} \right\}, \quad (72)$$

where  $\text{Im } \xi$  is a scalar represents either the isotropic electric or magnetic susceptibility and we write the eigen-decomposition of  $\text{Im } \Gamma_0$  as  $\text{Im } \Gamma_0 = \mathbb{V} \mathbb{V}^\dagger$ .

3. Isotropic *electric* material (electric scalar material, any incident field, any geometry): same form as Eqs. (70)–(72) with  $\psi_{\text{inc}}$  replaced by  $\mathbf{e}_{\text{inc}}$ , and  $\Gamma_0$  replaced by  $\mathbb{G}_0^{\text{EE}}$ . Eigenbasis  $\mathbb{V}$  is now defined by the eigendecomposition:  $\text{Im } \mathbb{G}_0^{\text{EE}} = \mathbb{V} \mathbb{V}^\dagger$ , with  $\mathbf{v}_i$  being the  $i$ -th column of  $\mathbb{V}$ .

- (a) For far field scattering, where the incident electric field  $\mathbf{e}_{\text{inc}}$  is characterized by the property  $\mathbf{e}_{\text{inc}} \in \text{Range}\{\text{Im } \mathbb{G}_0^{\text{EE}}\}$ , bounds in Eqs. (70)–(72) can be dramatically simplified:

**Far field incidence:**  
**electric scalar material, any shape**

$$P_{\text{ext}} \leq \frac{\omega}{2} \mathbf{e}_{\text{inc}}^\dagger (\text{Im } \xi + \text{Im } \mathbb{G}_0^{\text{EE}})^{-1} \mathbf{e}_{\text{inc}} \quad (73)$$

$$P_{\text{abs}} \leq \frac{\omega}{2} \frac{\nu^{*2}}{4} \mathbf{e}_{\text{inc}}^\dagger [(\nu^* - 1) \text{Im } \xi + \nu^* \text{Im } \mathbb{G}_0^{\text{EE}}]^{-1} \mathbf{e}_{\text{inc}} \quad (74)$$

$$P_{\text{scat}} \leq \frac{\omega}{2} \frac{\nu^{*2}}{4} \mathbf{e}_{\text{inc}}^\dagger [\nu^* \text{Im } \xi + (\nu^* - 1) \text{Im } \mathbb{G}_0^{\text{EE}}]^{-1} \mathbf{e}_{\text{inc}}. \quad (75)$$

- Plane wave incidence (applies to both finite and extended scatterers) with  $\mathbf{e}_{\text{inc}} = \sum_i e_i \mathbf{v}_i$ . Explicitly

written out contributions from different channels:

**Plane wave incidence:  
electric scalar material, any shape**

$$P_{\text{ext}} \leq \frac{\omega}{2} \sum_i |e_i|^2 \frac{\rho_i}{\text{Im } \xi + \rho_i} \quad (76)$$

$$P_{\text{abs}} \leq \frac{\omega}{2} \frac{\nu^{*2}}{4} \sum_i |e_i|^2 \frac{\rho_i}{(\nu^* - 1) \text{Im } \xi + \nu^* \rho_i} \quad (77)$$

$$P_{\text{scat}} \leq \frac{\omega}{2} \frac{\nu^{*2}}{4} \sum_i |e_i|^2 \frac{\rho_i}{\nu^* \text{Im } \xi + (\nu^* - 1) \rho_i}, \quad (78)$$

where  $\rho_i = \mathbf{v}_i^\dagger \mathbf{v}_i$  is analytically known for highly symmetric bounding volumes.

- VSW incidence (applies to finite scatterers). Now the incident field is one specific VSW:  $\mathbf{e}_{\text{inc}} = e_i \mathbf{v}_i$ , under which:

**VSW incidence: electric scalar material, any shape**

$$P_{\text{ext}} \leq \frac{\omega}{2} \frac{|e_i|^2}{\text{Im } \xi + \rho_i}$$

$$P_{\text{abs}} \leq \frac{\omega}{2} \frac{\nu^{*2}}{4} \frac{|e_i|^2}{(\nu^* - 1) \text{Im } \xi + \nu^* \rho_i} = \begin{cases} \frac{\text{Im } \xi}{(\text{Im } \xi + \rho_i)^2} |e_i|^2 & \text{if } \rho_i \leq \text{Im } \xi \\ \frac{1}{4\rho_i} |e_i|^2 & \text{if } \rho_i \geq \text{Im } \xi \end{cases}$$

$$P_{\text{scat}} \leq \frac{\omega}{2} \frac{\nu^{*2}}{4} \frac{|e_i|^2}{\nu^* \text{Im } \xi + (\nu^* - 1) \rho_i} = \begin{cases} \frac{\rho_i}{(\text{Im } \xi + \rho_{\text{max}})^2} |e_i|^2 & \text{if } \rho_i \geq \frac{\rho_{\text{max}} \text{Im } \xi}{2 \text{Im } \xi + \rho_{\text{max}}} \\ \frac{1}{4} \frac{\rho_{\text{max}}^2}{\text{Im } \xi (\rho_{\text{max}} + \text{Im } \xi) (\rho_{\text{max}} - \rho_i)} |e_i|^2 & \text{if } \rho_i \leq \frac{\rho_{\text{max}} \text{Im } \xi}{2 \text{Im } \xi + \rho_{\text{max}}}, \end{cases}$$

where the choice of  $\nu^*$  is simple enough that we can write out explicit two possible solutions of  $P_{\text{abs}}$  and  $P_{\text{scat}}$ . We denote the maximum in  $\{\rho_i\}$  as  $\rho_{\text{max}}$ .

- (b) Incident field in near-field scattering is not necessarily in the range of  $\text{Im } \mathbb{G}_0^{\text{EE}}$  as evanescent waves may contribute (for an extended scatter). Expression for its bound takes the most general form as Eqs. (70)–(72) with  $\psi_{\text{inc}}$  replaced by  $\mathbf{e}_{\text{inc}}$ , and  $\Gamma_0$  replaced by  $\mathbb{G}_0^{\text{EE}}$ . For arbitrary dipole sources  $\mathbf{p}$ , the incident field can be written as  $\mathbf{e}_{\text{inc}} = \mathbb{G}_{0,\mathbf{p} \rightarrow V}^{\text{EE}} \mathbf{p}$  where  $\mathbb{G}_{0,\mathbf{p} \rightarrow V}^{\text{EE}}$  is an integral Green's function mapped from the region of dipole source  $\mathbf{p}$  to the scatterer  $V$ . Taking the singular vector decomposition of  $\mathbb{G}_{0,\mathbf{p} \rightarrow V}^{\text{EE}} = \mathbf{U} \mathbf{W}^\dagger$ , bounds for near field scattering can be written as:

**Near field incidence: electric scalar material, any shape**

$$P_{\text{ext}} \leq \frac{\omega}{2} \frac{1}{\text{Im } \xi} \mathbf{p}^\dagger \mathbf{W} [\mathbf{U}^\dagger \mathbf{U} - \mathbf{U}^\dagger \mathbf{V} (\text{Im } \xi + \mathbf{V}^\dagger \mathbf{V})^{-1} \mathbf{V}^\dagger \mathbf{U}] \mathbf{W}^\dagger \mathbf{p}$$

$$= \frac{\omega}{2} \frac{1}{\text{Im } \xi} \sum_i |\mathbf{p}^\dagger \mathbf{w}_i|^2 \left( \mathbf{u}_i^\dagger \mathbf{u}_i - \frac{|\mathbf{u}_i^\dagger \mathbf{v}_i|^2}{\text{Im } \xi + \mathbf{v}_i^\dagger \mathbf{v}_i} \right) \quad (79)$$

$$P_{\text{abs}} \leq \frac{\omega}{2} \frac{\nu^{*2}}{4(\nu^* - 1)} \frac{1}{\text{Im } \xi} \mathbf{p}^\dagger \mathbf{W} \{ \mathbf{U}^\dagger \mathbf{U} - \mathbf{U}^\dagger \mathbf{V} [(\nu^* - 1) \text{Im } \xi / \nu^* + \mathbf{V}^\dagger \mathbf{V}]^{-1} \mathbf{V}^\dagger \mathbf{U} \} \mathbf{W}^\dagger \mathbf{p}$$

$$= \frac{\omega}{2} \frac{\nu^{*2}}{4(\nu^* - 1)} \frac{1}{\text{Im } \xi} \sum_i |\mathbf{p}^\dagger \mathbf{w}_i|^2 \left( \mathbf{u}_i^\dagger \mathbf{u}_i - \frac{|\mathbf{u}_i^\dagger \mathbf{v}_i|^2}{(\nu^* - 1) \text{Im } \xi / \nu^* + \mathbf{v}_i^\dagger \mathbf{v}_i} \right) \quad (80)$$

$$P_{\text{scat}} \leq \frac{\omega}{2} \frac{\nu^*}{4} \frac{1}{\text{Im } \xi} \mathbf{p}^\dagger \mathbf{W} \{ \mathbf{U}^\dagger \mathbf{U} - \mathbf{U}^\dagger \mathbf{V} [\nu^* \text{Im } \xi / (\nu^* - 1) + \mathbf{V}^\dagger \mathbf{V}]^{-1} \mathbf{V}^\dagger \mathbf{U} \} \mathbf{W}^\dagger \mathbf{p}$$

$$= \frac{\omega}{2} \frac{\nu^*}{4} \frac{1}{\text{Im } \xi} \sum_i |\mathbf{p}^\dagger \mathbf{w}_i|^2 \left( \mathbf{u}_i^\dagger \mathbf{u}_i - \frac{|\mathbf{u}_i^\dagger \mathbf{v}_i|^2}{\nu^* \text{Im } \xi / (\nu^* - 1) + \mathbf{v}_i^\dagger \mathbf{v}_i} \right). \quad (81)$$

## XI. BOUND FOR LOCAL DENSITY OF STATES (LDOS)

*a. General bounds for LDOS* We start with the expressions of total, non-radiative, radiative electric LDOS in their volume integral form [2]:

$$\rho_{\text{tot}} = \rho_0 + \frac{1}{\pi\omega} \sum_j \text{Im} \left( \tilde{\psi}_{\text{inc},j}^\dagger \phi_j \right) \quad (82)$$

$$\rho_{\text{nr}} = \frac{1}{\pi\omega} \sum_j \phi_j^\dagger (\text{Im} \xi) \phi_j \quad (83)$$

$$\rho_{\text{rad}} = \rho_0 + \frac{1}{\pi\omega} \sum_j \left[ \text{Im} \left( \tilde{\psi}_{\text{inc},j}^\dagger \phi_j \right) - \phi_j^\dagger (\text{Im} \xi) \phi_j \right], \quad (84)$$

where  $\rho_0$  is the electric LDOS of the background material, and takes the value of  $\frac{\omega^2}{2\pi^2 c^3}$  for a scatterer in the vacuum [14]. Summation  $j = 1, 2, 3$  denotes power quantities from three orthogonally polarized unit dipoles. Incident field from dipole  $j$  is denoted by  $\psi_{\text{inc},j} = (\mathbf{e}_{\text{inc},j}, \mathbf{h}_{\text{inc},j})$ . Here we use lowercase notations for both electric and magnetic fields to emphasize their vector nature, as opposed to capitalized characters that are usually reserved for operators and matrices. Such incident field excites polarization current  $\phi_j$  in the scatterer. Complex conjugate of  $\psi_{\text{inc},j}$  (with a minus sign in front of magnetic fields) is denoted by  $\tilde{\psi}_{\text{inc},j} = (\mathbf{e}_{\text{inc},j}^*, -\mathbf{h}_{\text{inc},j}^*)$ .

Because three dipoles are uncorrelated, we can first solve the bound for one unit dipole. For simplicity, we omit its index  $j$  and write its incident field as  $\psi_{\text{inc}}$ , which excites polarization current  $\phi$  in the body. For this dipole, its non-radiative LDOS can be bounded by maximum absorption in Eq. (18) by identifying the objective function as  $\phi^\dagger (\text{Im} \xi) \phi$ . Bounds on total and radiative LDOS are less straightforward and are discussed below.

Objective function for total LDOS is  $\text{Im} \left( \tilde{\psi}_{\text{inc}}^\dagger \phi \right)$  with energy conservation constraint  $\phi^\dagger (\text{Im} \xi + \text{Im} \Gamma_0) \phi = \text{Im} \left( \psi_{\text{inc}}^\dagger \phi \right)$ . This echos with Eq. (1) with  $\mathbb{A} = 0$  and  $\beta = \tilde{\psi}_{\text{inc}}$ . Its maximum is given by Eq. (7):

$$\max_{\phi} \left\{ \text{Im} \left( \tilde{\psi}_{\text{inc}}^\dagger \phi \right) \right\} = \frac{1}{4\nu^*} (\tilde{\psi}_{\text{inc}} + \nu^* \psi_{\text{inc}})^\dagger (\text{Im} \xi + \text{Im} \Gamma_0)^{-1} (\tilde{\psi}_{\text{inc}} + \nu^* \psi_{\text{inc}}), \quad (85)$$

where the optimal dual variable  $\nu^*$  is always chosen at  $\nu_1 > \nu_0 = 0$  given by Eq. (10):

$$\nu^* = \nu_1 = \left[ \frac{\tilde{\psi}_{\text{inc}}^\dagger (\text{Im} \xi + \text{Im} \Gamma_0)^{-1} \tilde{\psi}_{\text{inc}}}{\psi_{\text{inc}}^\dagger (\text{Im} \xi + \text{Im} \Gamma_0)^{-1} \psi_{\text{inc}}} \right]^{\frac{1}{2}}. \quad (86)$$

For non-magnetic scatterer, the above expression can be significantly simplified. No magnetic current can be excited in the non-magnetic scatterer such that  $\mathbf{M} = 0$ . Examining the object function  $\text{Im} \left( \tilde{\psi}_{\text{inc}}^\dagger \phi \right)$ , we can find that it is equivalent to set  $\mathbf{h}_{\text{inc}} = 0$ . Equation (86) gives  $\nu^* = 1$  and the maximum objective function for non-magnetic scatterer can be simplified to:

$$\max_{\phi} \left\{ \text{Im} \left( \tilde{\psi}_{\text{inc}}^\dagger \phi \right) \right\} = [\text{Re} \mathbf{e}_{\text{inc}}]^\dagger (\text{Im} \xi + \text{Im} \mathbb{G}_0^{\text{EE}})^{-1} [\text{Re} \mathbf{e}_{\text{inc}}] \quad (87)$$

$$\leq \mathbf{e}_{\text{inc}}^\dagger (\text{Im} \xi + \text{Im} \mathbb{G}_0^{\text{EE}})^{-1} \mathbf{e}_{\text{inc}} \quad (88)$$

$$= \frac{2}{\omega} P_{\text{ext}}^{\text{max}}. \quad (89)$$

where in the last two lines, we relax the bound to the maximum-extinction bound given in Eq. (14) with the same assumption of non-magnetic scatterer.

Objective function for radiative LDOS defined in Eq. (84) can be chosen as  $\text{Im} \left( \tilde{\psi}_{\text{inc}}^\dagger \phi \right) - \phi^\dagger (\text{Im} \xi) \phi$ . Thus,  $\mathbb{A} = -\text{Im} \xi$ ,  $\beta = \tilde{\psi}_{\text{inc}}$ . Maximal objective function given by Eq. (7) can be written as:

$$\max_{\phi} \left\{ \text{Im} \left( \tilde{\psi}_{\text{inc}}^\dagger \phi \right) - \phi^\dagger (\text{Im} \xi) \phi \right\} = \frac{1}{4} (\tilde{\psi}_{\text{inc}} + \nu^* \psi_{\text{inc}})^\dagger [(\nu^* + 1) \text{Im} \xi + \nu^* \text{Im} \Gamma_0]^{-1} (\tilde{\psi}_{\text{inc}} + \nu^* \psi_{\text{inc}}) \quad (90)$$

with optimal dual variable  $\nu^*$  given by Eq. (11). For non-magnetic scatterer (effectively  $\mathbf{h}_{\text{inc}} = 0$  in Eq. (90)), bound in Eq. (90) reduces to:

$$\max_{\phi} \left\{ \text{Im} \left( \tilde{\psi}_{\text{inc}}^\dagger \phi \right) - \phi^\dagger (\text{Im} \xi) \phi \right\} = \frac{1}{4} (\tilde{\mathbf{e}}_{\text{inc}} + \nu^* \mathbf{e}_{\text{inc}})^\dagger [(\nu^* + 1) \text{Im} \xi + \nu^* \text{Im} \mathbb{G}_0^{\text{EE}}]^{-1} (\tilde{\mathbf{e}}_{\text{inc}} + \nu^* \mathbf{e}_{\text{inc}}). \quad (91)$$



Radiative LDOS bound in Eq. (91) can be relaxed to scattering bound in Eq. (21) by observing that the dual function of the former,  $g_1(\nu)$ , is always greater than or equal to the latter (after suppressing its  $\frac{\omega}{2}$  factor),  $g_2(\nu)$ , for any  $\nu \geq \nu_0$ :

$$g_1(\nu) = -\frac{1}{4}(\tilde{\mathbf{e}}_{\text{inc}} + \nu \mathbf{e}_{\text{inc}})^\dagger [(\nu + 1) \text{Im } \xi + \nu \text{Im } \mathbb{G}_0^{\text{EE}}]^{-1} (\tilde{\mathbf{e}}_{\text{inc}} + \nu \mathbf{e}_{\text{inc}}) \quad (92)$$

$$\geq -\frac{(1 + \nu)^2}{4} \mathbf{e}_{\text{inc}}^\dagger [(\nu + 1) \text{Im } \xi + \nu \text{Im } \mathbb{G}_0^{\text{EE}}]^{-1} \mathbf{e}_{\text{inc}} = g_2(\nu). \quad (93)$$

The last inequality can be proved by performing Cholesky decomposition on the Hermitian operator  $[(\nu + 1) \text{Im } \xi + \nu \text{Im } \mathbb{G}_0^{\text{EE}}]^{-1} = \mathbb{L}^\dagger \mathbb{L}$  and using Cauchy–Schwarz inequality to relax the cross term:

$$\text{Re}\{\mathbf{e}_{\text{inc}}^\dagger \mathbb{L}^\dagger \mathbb{L} \mathbf{e}_{\text{inc}}^*\} \leq \left| \mathbf{e}_{\text{inc}}^\dagger \mathbb{L}^\dagger \mathbb{L} \mathbf{e}_{\text{inc}}^* \right| \leq \|\mathbb{L} \mathbf{e}_{\text{inc}}\| \cdot \|\mathbb{L} \mathbf{e}_{\text{inc}}^*\| = \|\mathbb{L} \mathbf{e}_{\text{inc}}\|^2 = \mathbf{e}_{\text{inc}}^\dagger \mathbb{L}^\dagger \mathbb{L} \mathbf{e}_{\text{inc}}. \quad (94)$$

It follows from Eq. (93) that the maximum of  $g_1(\nu)$  is greater than the maximum of  $g_2(\nu)$ . The optimum of a primal function is given by the negative of the maximum of a dual function, so the optimal objective function considered here is smaller than the optimal scattering bound in Eq. (21), and equivalently Eq. (20):

$$\max_{\phi} \left\{ \text{Im} \left( \tilde{\psi}_{\text{inc}}^\dagger \phi \right) - \phi^\dagger (\text{Im } \xi) \phi \right\} \leq \frac{2}{\omega} P_{\text{sca}}^{\text{max}}. \quad (95)$$

To summarize, we derive general LDOS bounds for any material. For non-magnetic material specifically, LDOS can be directly bounded by maximum power response in Eqs. (14), (18), and (20):

$$\rho_{\text{tot}} \leq \frac{2}{\pi \omega^2} \sum_j P_{\text{ext},j}^{\text{max}} + \rho_0 \quad (96)$$

$$\rho_{\text{nr}} \leq \frac{2}{\pi \omega^2} \sum_j P_{\text{abs},j}^{\text{max}} \quad (97)$$

$$\rho_{\text{rad}} \leq \frac{2}{\pi \omega^2} \sum_j P_{\text{sca},j}^{\text{max}} + \rho_0, \quad (98)$$

where  $j = 1, 2, 3$  denotes the summation of maximum power quantities from three orthogonally polarized unit dipoles.

*b. LDOS bounds for a finite non-magnetic scatterer* In the following, we assume the scatterer is non-magnetic and finite, embedded in the vacuum. The non-magnetic nature of the scatterer allows us to use Eqs. (96)–(98) to decompose LDOS bounds to previous power bounds for three orthogonally polarized unit dipoles. In Eqs. (79)–(81), we presented power bounds for arbitrary dipole distributions  $\mathbf{p}(\mathbf{x})$ . Here, we start with a point dipole oriented along  $\hat{\mathbf{e}}_j$  at origin  $\mathbf{p}(\mathbf{x}) = \mathbf{p}_j(\mathbf{x}) = p_0 \delta(\mathbf{x}) \hat{\mathbf{e}}_j$  with  $p_0 = 1$ , and later sum up the contributions from three orthogonal polarizations. We also assume the scatterer is finite, thus can be enclosed by a spherical shell (see Fig. 2 inset). A shell-like bounding volume has spherical symmetry, so  $\mathbf{v}_i$  and  $\mathbf{w}_i$  in Eqs. (79)–(81) are regular VSWs:

$$\mathbf{v}_{mn1}(\mathbf{x}) = \mathbf{w}_{mn1}(\mathbf{x}) = k^{\frac{3}{2}} R g \mathbf{M}_{mn}(kr, \theta, \phi) \quad (99)$$

$$\mathbf{v}_{mn2}(\mathbf{x}) = \mathbf{w}_{mn2}(\mathbf{x}) = k^{\frac{3}{2}} R g \mathbf{N}_{mn}(kr, \theta, \phi), \quad (100)$$

$\mathbf{u}_i$  are outgoing VSWs:

$$\mathbf{u}_{mn1}(\mathbf{x}) = k^{\frac{3}{2}} \mathbf{M}_{mn}(kr, \theta, \phi) \quad (101)$$

$$\mathbf{u}_{mn2}(\mathbf{x}) = k^{\frac{3}{2}} \mathbf{N}_{mn}(kr, \theta, \phi). \quad (102)$$

Power bounds in Eqs. (79)–(81) require us to evaluate four overlap integrals:  $\mathbf{p}_j^\dagger \mathbf{w}_i, \mathbf{u}_i^\dagger \mathbf{u}_i, \mathbf{u}_i^\dagger \mathbf{v}_i, \mathbf{v}_i^\dagger \mathbf{v}_i$ . We first evaluate overlap integral between the point dipole and regular VSWs in the source volume  $V_s$ :

$$\mathbf{p}_j^\dagger \mathbf{w}_i = \int_{V_s} \mathbf{p}_j^*(\mathbf{x}) \cdot \mathbf{w}_i(\mathbf{x}) d\mathbf{x} \quad (103)$$

$$= p_0 \hat{\mathbf{e}}_j \cdot \mathbf{w}_i(\mathbf{x} = 0) \quad (104)$$

$$= k^{\frac{3}{2}} p_0 \begin{cases} \mathbf{e}_j \cdot R g \mathbf{N}_{m,1}(0, \theta, \phi) & \text{if } j = 2, n = 1 \\ 0 & \text{else,} \end{cases} \quad (105)$$

where we used the fact that only  $Rg\mathbf{N}_{m,1}$  has nonzero value at the origin. Exact value of the dot product  $\mathbf{e}_j \cdot Rg\mathbf{N}_{m,1}(0, \theta, \phi)$  depends on the orientation of the dipole:

$$\mathbf{e}_j \cdot Rg\mathbf{N}_{m,1}(0, \theta, \phi) = \begin{cases} \pm \frac{1}{2\sqrt{3}\pi} \delta_{m,\pm 1} & \text{if } \hat{\mathbf{e}}_j = \hat{\mathbf{x}} \\ \frac{1}{2i\sqrt{3}\pi} \delta_{m,\pm 1} & \text{if } \hat{\mathbf{e}}_j = \hat{\mathbf{y}} \\ -\frac{1}{\sqrt{6}\pi} \delta_{m,0} & \text{if } \hat{\mathbf{e}}_j = \hat{\mathbf{z}}. \end{cases} \quad (106)$$

Later for LDOS, we will need to evaluate averaged power from three randomly oriented dipoles, which is related to the quantity:

$$\frac{1}{3} \sum_j |\mathbf{p}_j^\dagger \mathbf{w}_i|^2 = k^3 \frac{p_0^3}{18\pi} \delta_{n,1} \delta_{j,2}, \quad (107)$$

where  $\hat{\mathbf{e}}_j$  runs through directions  $\hat{\mathbf{x}}$ ,  $\hat{\mathbf{y}}$ , and  $\hat{\mathbf{z}}$ . We now evaluate overlap integrals between different VSWs within the bounding volume  $V$ :

$$\mathbf{v}_i^\dagger \mathbf{v}_i = \int_V \mathbf{v}_{mnj}^*(\mathbf{x}) \cdot \mathbf{v}_{mnj}(\mathbf{x}) d\mathbf{x} = I_j \left( j_n^{(1)}(x), j_n^{(1)}(x) \right) \quad (108)$$

$$\mathbf{u}_i^\dagger \mathbf{u}_i = \int_V \mathbf{u}_{mnj}^*(\mathbf{x}) \cdot \mathbf{u}_{mnj}(\mathbf{x}) d\mathbf{x} = I_j \left( h_n^{(1)*}(x), h_n^{(1)}(x) \right) \quad (109)$$

$$\mathbf{u}_i^\dagger \mathbf{v}_i = \int_V \mathbf{u}_{mnj}^*(\mathbf{x}) \cdot \mathbf{v}_{mnj}(\mathbf{x}) d\mathbf{x} = I_j \left( h_n^{(1)*}(x), j_n^{(1)}(x) \right), \quad (110)$$

where we defined function:

$$I_j \left( z_n^{(1)}(x), z_n^{(2)}(x) \right) = \begin{cases} \int_{kR_1}^{kR_2} x^2 z_n^{(1)}(x) z_n^{(2)}(x) dx & \text{if } j = 1 \\ n(n+1) \int_{kR_1}^{kR_2} z_n^{(1)}(x) z_n^{(2)}(x) dx + \int_{kR_1}^{kR_2} [x z_n^{(1)}(x)]' [x z_n^{(2)}(x)]' dx & \text{if } j = 2. \end{cases} \quad (111)$$

Bound for total extinction from three randomly oriented dipoles is bounded by:

$$\frac{1}{3} \sum_j P_{\text{ext},j} \leq \frac{1}{3} \sum_j \sum_i \frac{\omega}{2} |\mathbf{p}_j^\dagger \mathbf{w}_i|^2 \underbrace{\frac{1}{\text{Im} \xi} \left( \mathbf{u}_i^\dagger \mathbf{u}_i - \frac{|\mathbf{u}_i^\dagger \mathbf{v}_i|^2}{\text{Im} \xi + \mathbf{v}_i^\dagger \mathbf{v}_i} \right)}_{f_i}, \quad (112)$$

where we defined enhancement factor  $f_i$  (depends only on  $n$  and  $j$ ). Using Eq. (107), we can show that:

$$\frac{\frac{1}{3} \sum_j P_{\text{ext},j}}{P_0} \leq f_{n=1,j=2}, \quad (113)$$

where  $P_0 = \omega k^3 p_0^3 / 12\pi$  is the power radiated by a dipole with amplitude  $p_0$  in vacuum. Similarly, one can show that:

$$\frac{\rho_{\text{tot}}}{\rho_0} \leq 1 + f_{n=1,j=2}. \quad (114)$$

The enhancement factor  $f_{n=1,j=2}$  shows how large the light extinction of three uncorrelated dipoles can be, compared to the vacuum. While the first term in Eq. (112) appears in previous material-loss bound [2], the second term comes from radiation coupling between the bounding volume and the vacuum. In near field when material loss dominates,  $f_{n=1,j=2}$  can be simplified to the material-loss bound:

$$f_{n=1,j=2} = \frac{1}{\text{Im} \xi} \mathbf{u}_i^\dagger \mathbf{u}_i \quad (115)$$

$$= \frac{1}{\text{Im} \xi} \left( x - \frac{1}{x} - \frac{1}{x^3} \right) \bigg|_{kR_1}^{kR_2} \quad (116)$$

$$\rightarrow \frac{1}{\text{Im} \xi} \frac{1}{k^3 R_1^3}, \quad (117)$$

where, in the last line, we take the limit of extreme near field where  $kR_1 \ll 1, kR_2$ . In Fig. 2, we showed the general bound and material-loss bound for LDOS enhancement at wavelength 360 nm by Ag surroundings. It is clear that

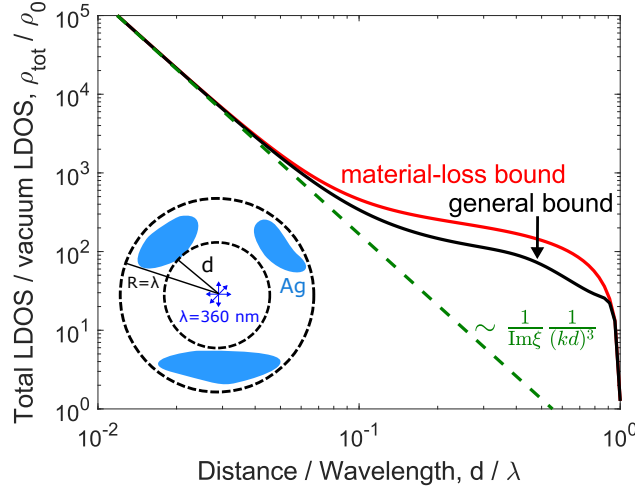


FIG. 2. Bounding volume for the LDOS problem is chosen to be a spherical shell with three randomly oriented dipoles in the center, radiating at wavelength  $\lambda = 360$  nm. Inner radius of the shell is determined by the minimum distance  $d$  to the scatterer comprising only Ag. Outer radius  $R$  of the shell covers the far end of the scatterer and is assumed to be one wavelength in the figure. In the far field, general bound is tighter than material-loss bound. In the near field, general bound converge to material-loss bound, and both follow the same divergence as  $\frac{1}{\text{Im}\xi} \frac{1}{k^3 d^3}$ .

both bounds follow Eq. (117) in near field limit. In far field, general bound is slightly tighter than the material-loss bound due to the consideration of additional radiative loss.

Absorption and scattering bounds can also be written through an enhancement factor over the vacuum radiation:

$$\frac{\frac{1}{3} \sum_j P_{\text{abs}, \mathbf{p}_j}}{P_0} \leq f_{n=1, j=2}^{\text{abs}}(\nu^*) \quad (118)$$

$$\frac{\frac{1}{3} \sum_j P_{\text{sca}, \mathbf{p}_j}}{P_0} \leq f_{n=1, j=2}^{\text{sca}}(\nu^*). \quad (119)$$

Though they are more complicated in the sense that both enhancement factors (defined below) are functions of  $\nu^*$ , the optimal dual variable. Similarly, for non-radiative and radiative LDOS we can write:

$$\frac{\rho_{\text{nr}}}{\rho_0} \leq f_{n=1, j=2}^{\text{abs}}(\nu^*) \quad (120)$$

$$\frac{\rho_{\text{rad}}}{\rho_0} \leq 1 + f_{n=1, j=2}^{\text{sca}}(\nu^*). \quad (121)$$

Lastly, we present the explicit expressions of absorptive and scattering enhancement factors. For absorption, the enhancement factor is:

$$f_{n=1, j=2}^{\text{abs}}(\nu^*) = \frac{\nu^{*2}}{4(\nu^* - 1)} \frac{1}{\text{Im}\xi} \left( \mathbf{u}_i^\dagger \mathbf{u}_i - \frac{|\mathbf{u}_i^\dagger \mathbf{v}_i|^2}{(\nu^* - 1) \text{Im}\xi / \nu^* + \mathbf{v}_i^\dagger \mathbf{v}_i} \right),$$

where  $\nu^*$  is determined by solving  $a = (\nu^* - 1) \text{Im}\xi / \nu^*$  in the following equation:

$$2a \left( \mathbf{u}_i^\dagger \mathbf{u}_i - \frac{|\mathbf{u}_i^\dagger \mathbf{v}_i|^2}{a + \mathbf{v}_i^\dagger \mathbf{v}_i} \right) = \left\{ \mathbf{u}_i^\dagger \mathbf{u}_i \text{Im}\xi + |\mathbf{u}_i^\dagger \mathbf{v}_i|^2 \left[ 1 - \frac{(\text{Im}\xi + \mathbf{v}_i^\dagger \mathbf{v}_i)(2a + \mathbf{v}_i^\dagger \mathbf{v}_i)}{(a + \mathbf{v}_i^\dagger \mathbf{v}_i)^2} \right] \right\}.$$

For scattering, the enhancement factor is:

$$f_{n=1, j=2}^{\text{sca}}(\nu^*) = \frac{\nu^*}{4} \frac{1}{\text{Im}\xi} \left( \mathbf{u}_i^\dagger \mathbf{u}_i - \frac{|\mathbf{u}_i^\dagger \mathbf{v}_i|^2}{\nu^* \text{Im}\xi / (\nu^* - 1) + \mathbf{v}_i^\dagger \mathbf{v}_i} \right),$$

where  $\nu^*$  is determined by solving  $a = \nu^* \text{Im} \xi / (\nu^* - 1)$  in the following equation:

$$2 \text{Im} \xi \left( \mathbf{u}_i^\dagger \mathbf{u}_i - \frac{|\mathbf{u}_i^\dagger \mathbf{v}_i|^2}{a + \mathbf{v}_i^\dagger \mathbf{v}_i} \right) = \left\{ \mathbf{u}_i^\dagger \mathbf{u}_i \text{Im} \xi + |\mathbf{u}_i^\dagger \mathbf{v}_i|^2 \left[ 1 - \frac{(\text{Im} \xi + \mathbf{v}_i^\dagger \mathbf{v}_i)(2a + \mathbf{v}_i^\dagger \mathbf{v}_i)}{(a + \mathbf{v}_i^\dagger \mathbf{v}_i)^2} \right] \right\}.$$

- 
- [1] S. Boyd and L. Vandenberghe, *Convex optimization* (Cambridge university press, 2004).
  - [2] O. D. Miller, A. G. Polimeridis, M. H. Reid, C. W. Hsu, B. G. DeLacy, J. D. Joannopoulos, M. Soljačić, and S. G. Johnson, Fundamental limits to optical response in absorptive systems, *Optics express* **24**, 3329 (2016).
  - [3] L. Novotny and B. Hecht, *Principles of nano-optics* (Cambridge university press, 2012).
  - [4] J.-P. Hugonin, M. Besbes, and P. Ben-Abdallah, Fundamental limits for light absorption and scattering induced by cooperative electromagnetic interactions, *Physical Review B* **91**, 180202 (2015).
  - [5] R. E. Hamam, A. Karalis, J. Joannopoulos, and M. Soljačić, Coupled-mode theory for general free-space resonant scattering of waves, *Physical review A* **75**, 053801 (2007).
  - [6] D.-H. Kwon and D. M. Pozar, Optimal characteristics of an arbitrary receive antenna, *IEEE Transactions on Antennas and Propagation* **57**, 3720 (2009).
  - [7] Z. Ruan and S. Fan, Design of subwavelength superscattering nanospheres, *Applied Physics Letters* **98**, 043101 (2011).
  - [8] I. Liberal, Y. Ra'di, R. Gonzalo, I. Ederra, S. A. Tretyakov, and R. W. Ziolkowski, Least upper bounds of the powers extracted and scattered by bi-anisotropic particles, *IEEE Transactions on Antennas and Propagation* **62**, 4726 (2014).
  - [9] S. Molesky, W. Jin, P. S. Venkataram, and A. W. Rodriguez, T operator bounds on angle-integrated absorption and thermal radiation for arbitrary objects, *Physical Review Letters* **123**, 257401 (2019).
  - [10] W. L. Stutzman and G. A. Thiele, *Antenna theory and design*, 3rd ed. (John Wiley & Sons, 2012).
  - [11] L. Tsang, J. A. Kong, and K.-H. Ding, *Scattering of electromagnetic waves: theories and applications*, Vol. 27 (John Wiley & Sons, 2004).
  - [12] J. K. Bloomfield, S. H. Face, and Z. Moss, Indefinite integrals of spherical bessel functions, *arXiv preprint arXiv:1703.06428* (2017).
  - [13] M. Krüger, G. Bimonte, T. Emig, and M. Kardar, Trace formulas for nonequilibrium casimir interactions, heat radiation, and heat transfer for arbitrary objects, *Physical Review B* **86**, 115423 (2012).
  - [14] K. Joulain, J.-P. Mulet, F. Marquier, R. Carminati, and J.-J. Greffet, Surface electromagnetic waves thermally excited: Radiative heat transfer, coherence properties and casimir forces revisited in the near field, *Surface Science Reports* **57**, 59 (2005).